Ocean Engineering 344 (2026) 123705

Contents lists available at ScienceDirect

Ocean Engineering

journal homepage: www.elsevier.com/locate/oceaneng

Research paper

Numerical study on the leakage characteristic of the damaged LNG carrier in different wind scenarios

XinLong Zhang [a], QingYi Qu [a], Simone Mancini [b,*], Li Lin [c,d], YiHua Su [c,d], RenQing Zhu [a]

[a] School of Naval Architecture and Ocean Engineering, Jiangsu University of Science and Technology, Zhenjiang, 212000, China
[b] Department of Industrial Engineering, University of Naples "Federico II", Via Claudio 21, Naples, 80125, Italy
[c] Shanghai Rules and Research Institute, China Classification Society, Shanghai, 200135, China
[d] Ships and Offshore Installations Structural Safety Laboratory, China Classification Society, Shanghai, 200135, China

ARTICLE INFO

Keywords:
LNG carrier
Rapid phase transition
Leakage process
Rescue management
Disaster prevention

ABSTRACT

Leakage accidents on an LNG (Liquefied Natural Gas) carrier pose a significant threat to the safety of ship's structures and rescue personnel. This paper proposes a numerical approach by combining CFD (Computational Fluid Dynamics) and VOF (Volume of Fluid) boiling modules. This approach simulates the RPT (Rapid Phase Transition) behavior of cryogenic liquid cargo and dynamically visualizes the density field, temperature field, and diffusion range of the phase transition gas in the leakage process. Numerical convergence is verified based on the mesh and time-step sensitivity analysis conducted in the no-wind condition. Four additional scenarios including two beam wind directions, head wind, and following winds are applied to investigate effects of wind direction on the leakage characteristics. From the perspective of rescue management and disaster prevention, beam winds towards the damaged side represent the most dangerous scenarios, high methane concentration around the hull would increase the explosion risk while large cryogenic diffusion would reduce the safety of cargo tanks. Therefore, it is necessary to adjust the relative direction of the damaged LNG carrier to avoid being in this wind direction. Moreover, considering the safety of emergency personnel, the operation region should be positioned in the upwind area.

1. Introduction

Liquefied natural gas, as an important part of the global clean energy strategy, plays a vital role in international trade (Al-Yafei et al., 2021). The LNG carrier is the main method to transport liquefied natural gas from production terminals to consumption markets. Its safety is directly related to environmental protection, human life safety and global energy supply. Since liquefied natural gas is transported under cryogenic and high-pressure conditions, once the LNG carrier sustains damage, cryogenic LNG may transiently evaporate, forming a low-temperature cloud. This could potentially lead to extreme catastrophes such as fire and explosion (Nubli et al., 2022). Additionally, the resulting phase transition gas and diffusion behavior will produce complex temperature and pressure changes, posing a great threat to the safety of the ship structure and personnel (Nubli et al., 2024).

Fig. 1 shows a collision scenario between a Maltese "Aseem" LNG carrier and a China Hong-Kong "Shinyo Ocean" VLGC (Very Large Gas Carrier) ship. According to the accident report, both the VLGC and the LNG carrier suffered varying degrees of hull damage. Although the damage did not result in a leakage of LNG, it is sufficient to indicate the possibility of a cargo leakage during the voyage. Therefore, studying the characteristics of a potential leakage following such damage is of practical engineering value.

Cryogenic LNG leakage can cause severe economic losses and endanger human life. To ensure the ship's safety and improve risk control, many researchers have already made significant progress in analyzing the characteristics of LNG leakage (Giannissi et al., 2013; Kim et al., 2014; Yang and Pan, 2015). Numerous classical experimental campaigns have also been conducted to understand the leakage behavior, e.g., Esso tests, Shell Jet tests, Maplin Sands tests, Burro tests and Falcon tests (Koopman et al., 1982; Luketa-Hanlin, 2006). In recent years, Zhang et al. (2020) have conducted controlled experiments where LNG was released from a cryogenic storage tank. The aim was to analyze the dynamic behavior of LNG jets under water and vapor dispersion characteristics. Zhu et al. (2020) experimentally measured the vapor clouds and LNG concentration in the leakage accident. By depleting 1.4t

* Corresponding author.
E-mail address: simone.mancini@unina.it (S. Mancini).

https://doi.org/10.1016/j.oceaneng.2025.123705
Received 7 October 2025; Received in revised form 13 November 2025; Accepted 23 November 2025
Available online 27 November 2025

Fig. 1. Collision scenario between "Aseem" LNG carrier and "Shinyo Ocean" VLGC ship.

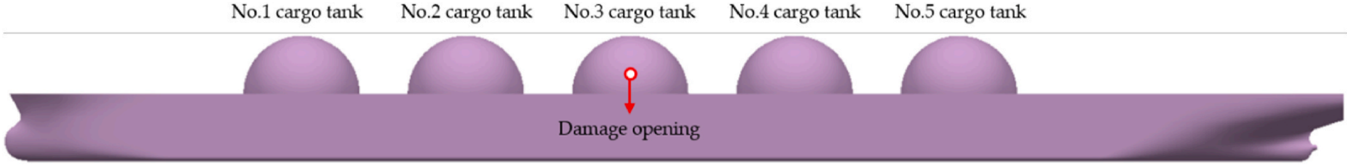

Fig. 2. Schematic diagram of the damaged LNG carrier.

LNG, the leakage diffusion rules are analyzed. Zhang et al. (2024) carried out the large-scale field experiment to cover LNG leakage pool with high expansion foam. The temperature and concentration changes of methane vapor at different locations were recorded and analyzed. In fact, field experiments can provide intuitive knowledge of physical phenomena. However, the relevant operations are highly dangerous. Additionally, the experimental results are susceptible to weather conditions, resulting in a low reproducibility.

Motivated by these consideration, qualitative and quantitative risk assessment (QRA) methodologies have been undertaken to study the leakage risks (George et al., 2019; Zhu et al., 2021; Kang et al., 2025). Yu et al. (2024) proposed a modified failure mode and effect analysis (FMEA) approach for qualitative risk assessment of LNG storage leakage. To quantify the probability and consequences of leakage risks more accurately, Xie et al. (2022) proposed an integrated QRA model for analyzing the fuel leakage risk during lockage of LNG-fueled ship, demonstrating that the main threat of LNG leakage is heat radiation rather than overpressure. These risk assessment frameworks are substantially valuable to support leakage prevention. However, methodologies solely evaluate the leakage risk from a static perspective and lack the capacity to dynamically capture the natural leakage in the real damage accident.

Table 1
Main particulars of the ship model.

Parameters	Particulars	Values
Length between perpendiculars	L_{pp} (m)	231.51
Breadth at Waterline	B_{WL} (m)	24.48
Depth	D (m)	11.8
Full load draft	T (m)	7.6
Diameter of the cargo tank	Φ (m)	20.5
Diameter of the damage opening	Φ (m)	1.6
Center of damage opening	(X, Y, Z) (m)	(120, 9.62, 15.3)

In recent years, with the development of high-performance computer, numerical simulations based on CFD have gained popularity to analyze the leakage characteristics (Choi et al., 2016), which can realize the actual leakage scenario and present the field details. Horvat (2018) developed a CFD methodology to simulate the behavior of LNG leakage from the initial release, spreading on the water surface, Rapid Phase Transition (RPT) to subsequent dispersion. The presented results demonstrate its capability of calculating the volume and distribution of flammable cloud, and the overpressure generated by an RPT event. Wu et al. (2021) proposed CFD and EnKF (Ensemble Kalman filter) coupling model to predict LNG vapor dispersion and estimate the strength of the LNG leakage source. Numerical results indicate that the leakage velocity can be obtained with acceptable errors after a period of data assimilation. Cao et al. (2022) employed the CFD software FLACS to establish the model of an on-deck LNG fuel area for the LNG-power Aframax oil tanker. It presents the distribution of potentially hazardous areas based on the concentration field and temperature field. Typical scenarios such as hose ruptures and valve joint leakages are investigated using the same FLACS software in LNG Ship-to-Ship Bunkering by Kong et al. (2023).

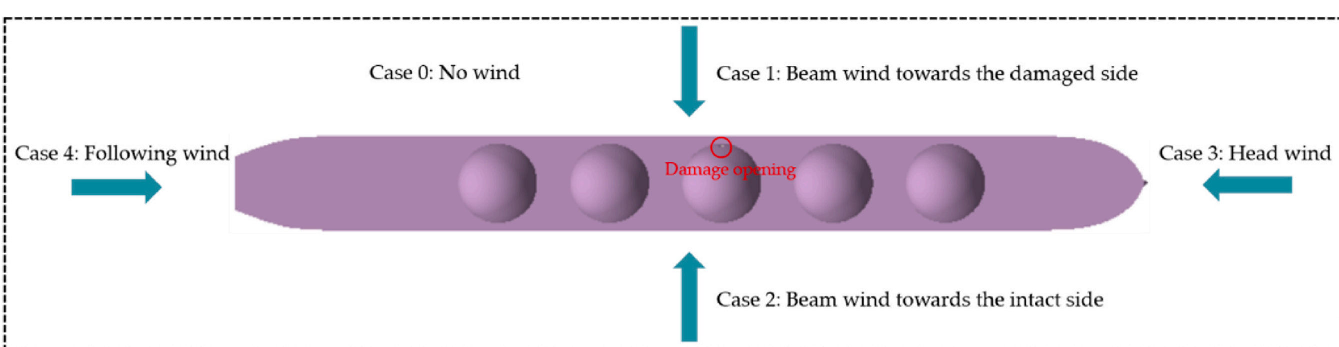

Fig. 3. Five simulation cases.

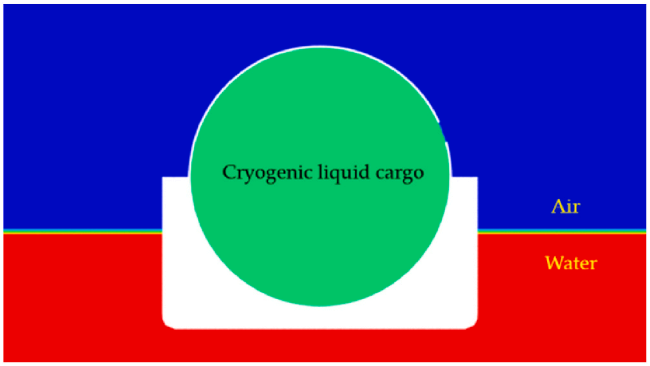

Fig. 4. Initial distribution of multiphase fluids.

Table 2
Initial physic properties of the four fluid phases.

Fluid phase	Water	Air	LNG	Phase-transition gas (CH4)
Density *[kg/ m³]*	997.561	1.184	430	0.657
Dynamic viscosity *[Pa· s]*	8.89×10^{-4}	1.86×10^{-5}	1.5×10^{-4}	1.12×10^{-5}
Temperature *[K]*	278	306	111	None

The dispersion range of the combustible vapor cloud is analyzed under both ballast and laden conditions.

Generally, although the numerical simulations above can well capture the leakage process, they are mostly based on the assumption that the leakage is controlled by specifying the mass rate at the damage section. The actual natural leakage cannot be simulated. Therefore, the first aim of this paper is to combine CFD models to form an efficient numerical approach that can simulate the natural leakage of cryogenic liquid cargo. Meanwhile, this approach can also provide the visualization of the density, temperature, and volume fraction of scalar fields, allowing for an analysis of the LNG leakage process and diffusion characteristics of the phase transition gas at a micro level. Moreover, the current research is mostly based on a single tank. Therefore, the second aim of this paper is to investigate the damaged LNG carrier under the premise of considering the actual hull shape and cargo tank arrangement. This is achieved by visualizing the temperature details on the hull surface and analyzing the diffusion process of the cryogenic phase transition gas on the hull deck, investigating effect of wind and its direction in the real scenario on the leakage characteristics. The results can provide optimization suggestions for the safety design of the deck structure and the enclosure protection of the cargo tank.

Based on the above considerations, this paper is focused on studying the leakage and diffusion of the mixed gas-liquid during the natural

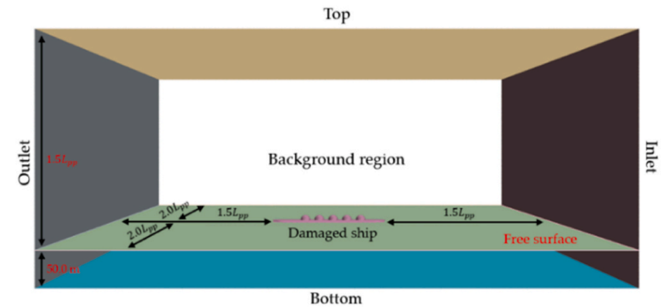

Fig. 6. Simulation domain and boundary condition.

Table 3
Boundary conditions.

Boundaries	Boundary condition
Inlet	Velocity inlet
Outlet	Pressure outlet
Top	Velocity inlet
Bottom	Velocity inlet
Sides	Symmetry plane

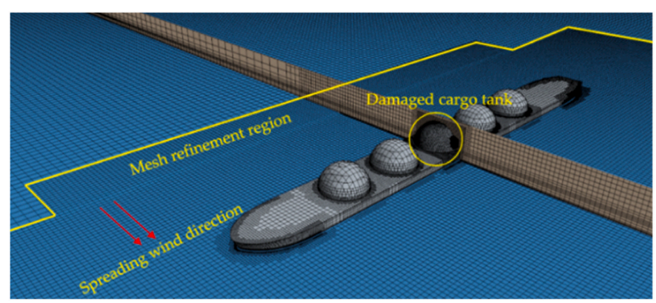

Fig. 7. Schematic diagram of the mesh generation.

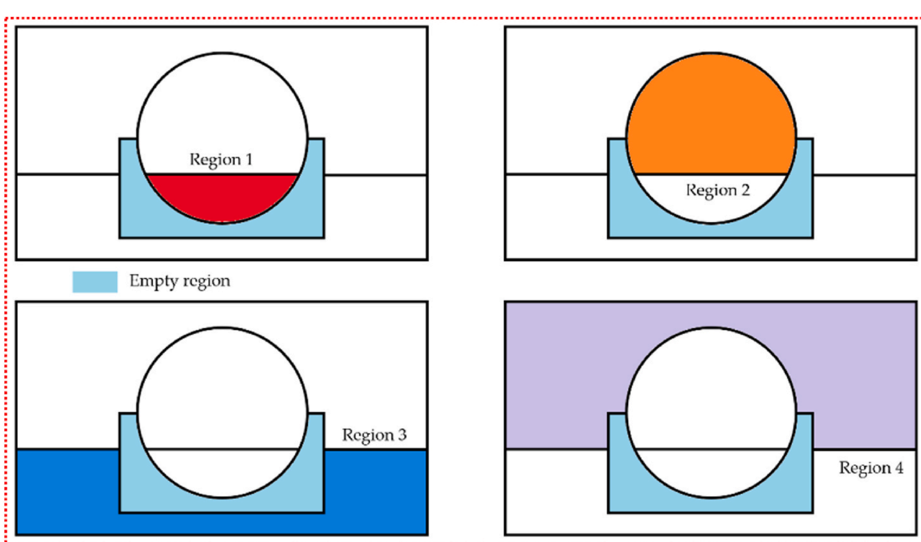

Fig. 5. Region division under the UDF function.

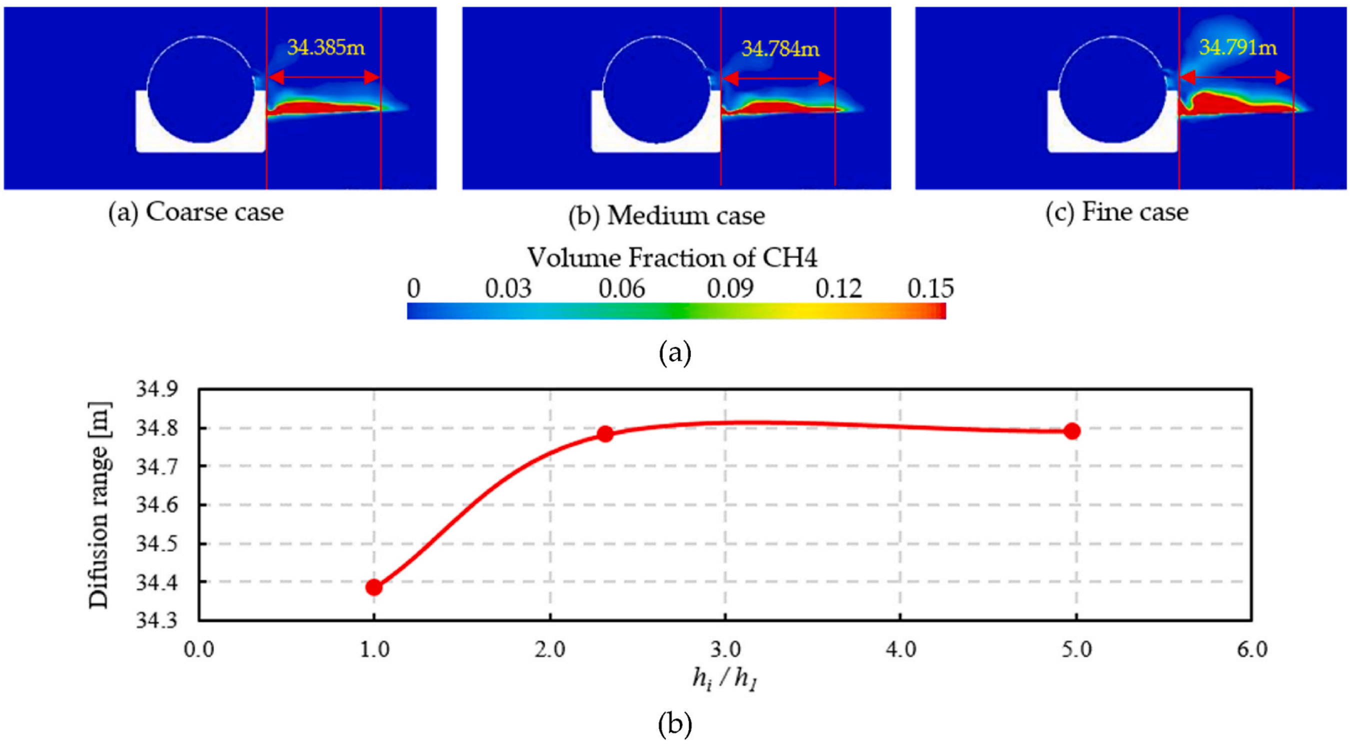

Fig. 8. (a) Mesh sensitivity analysis - maximum diffusion range of a 15 % concentration of methane at 5s after a leakage in the three mesh cases, **(b)** convergence trend for the three mesh cases.

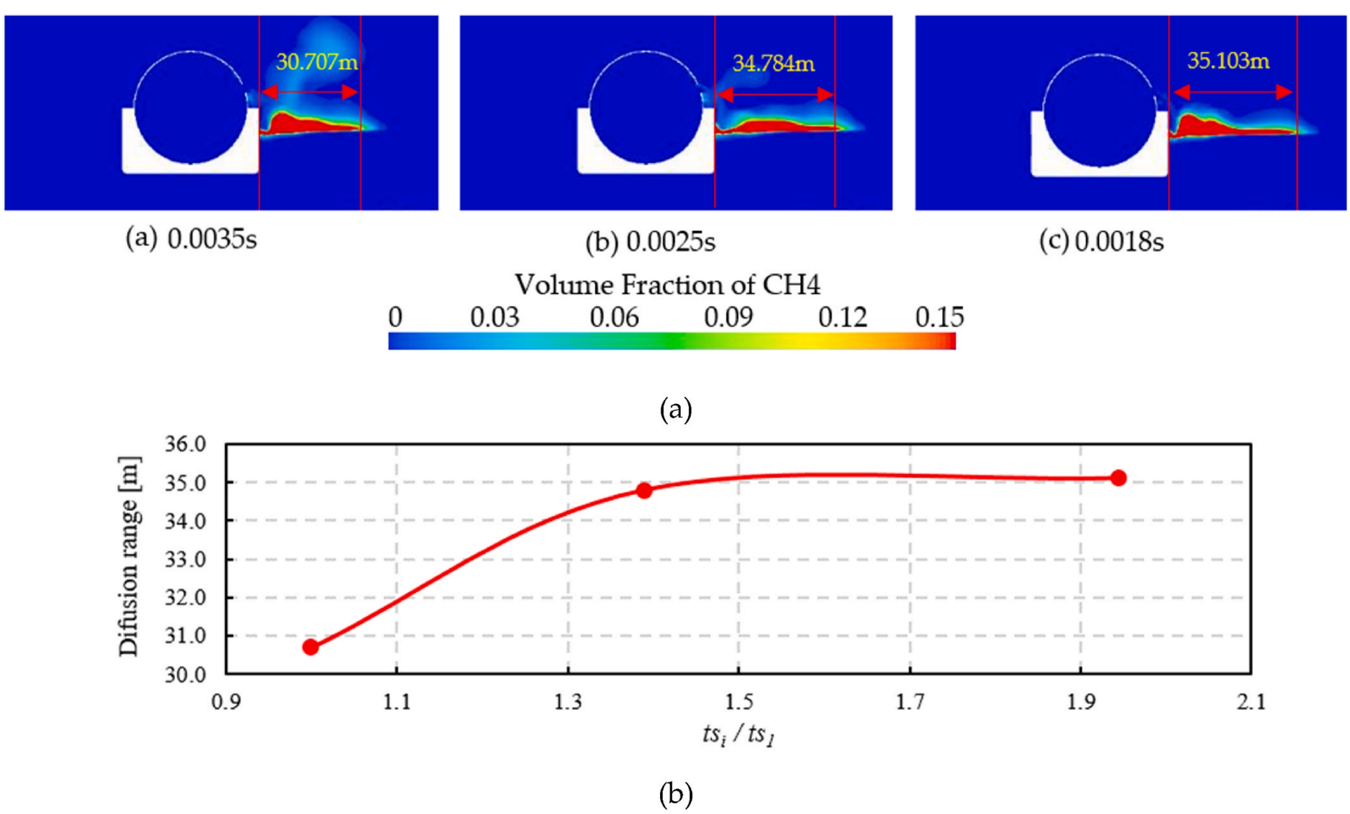

Fig. 9. (a) Time-step sensitivity analysis - maximum diffusion range of a 15 % concentration of methane at 5s after a leakage in the three time-step cases, **(b)** convergence trend for the three time step cases.

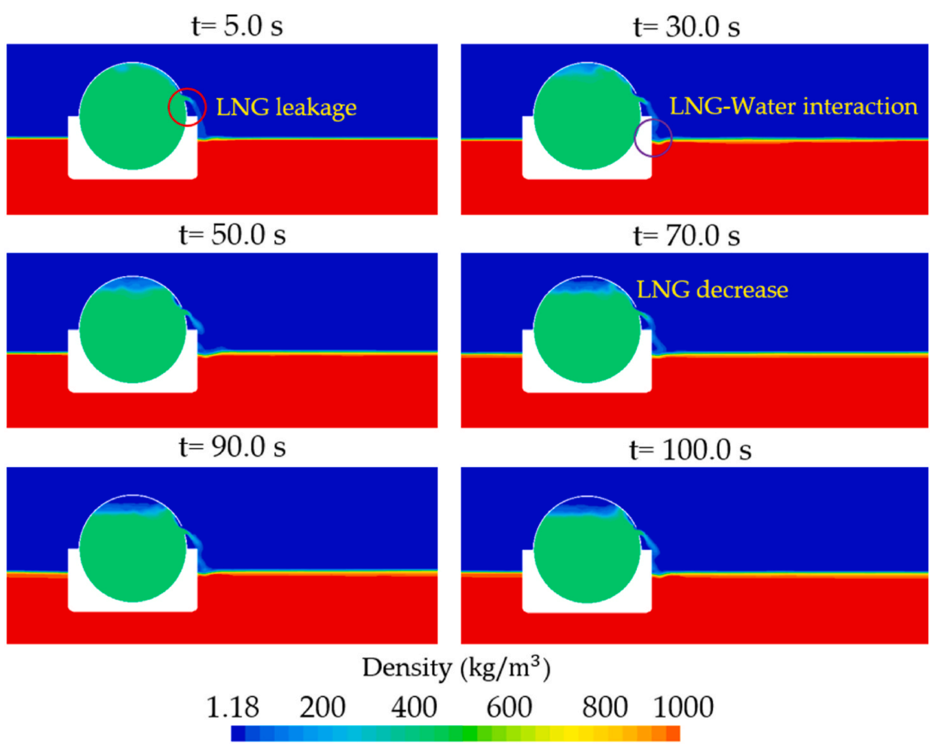

Fig. 10. Dynamic leakage process in the beam wind towards the damaged side of LNG carrier.

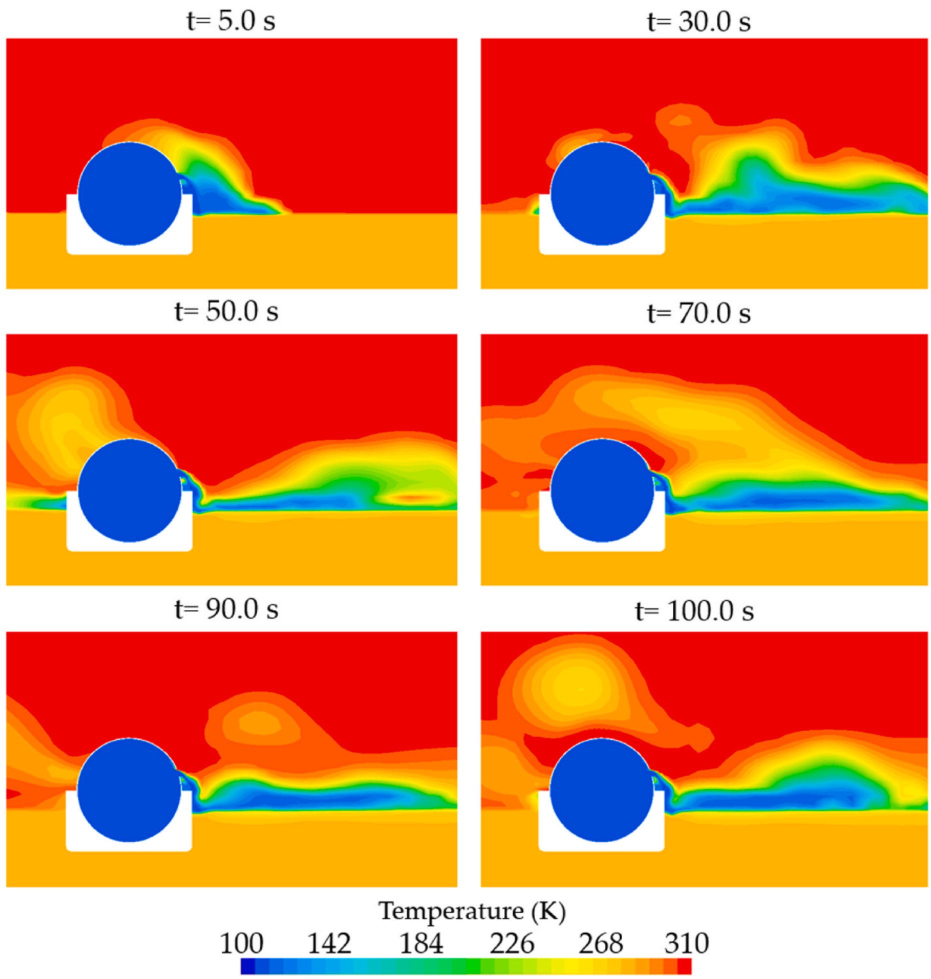

Fig. 11. Temperature field in the beam wind towards the damaged side of LNG carrier.

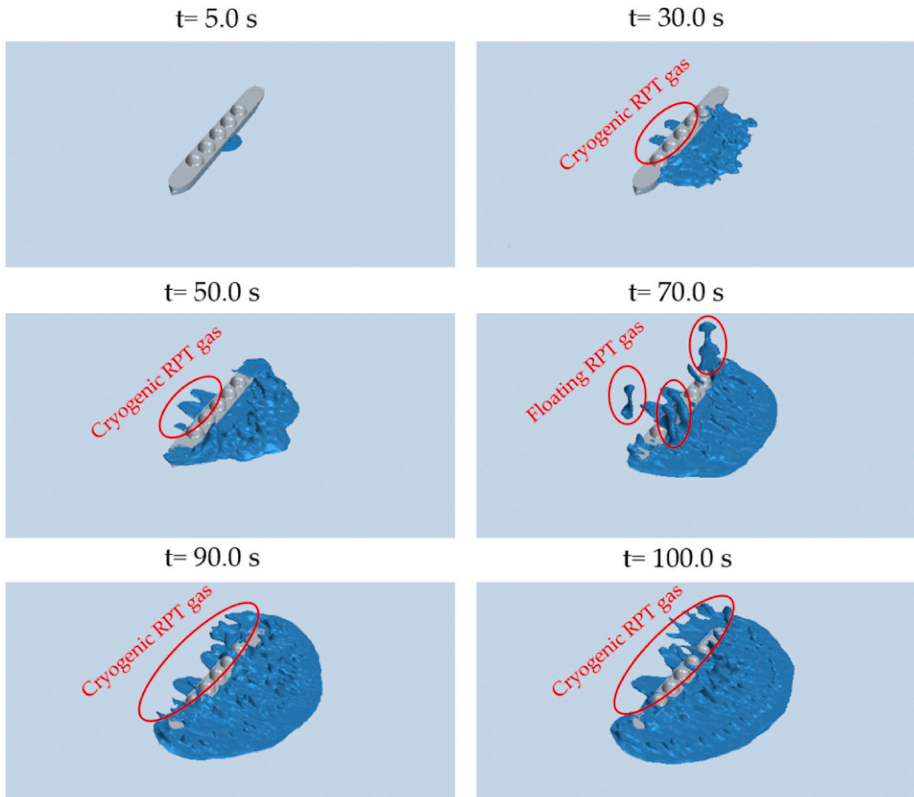

Fig. 12. Diffusion behavior of RPT gas in the beam wind towards the damaged side of LNG carrier.

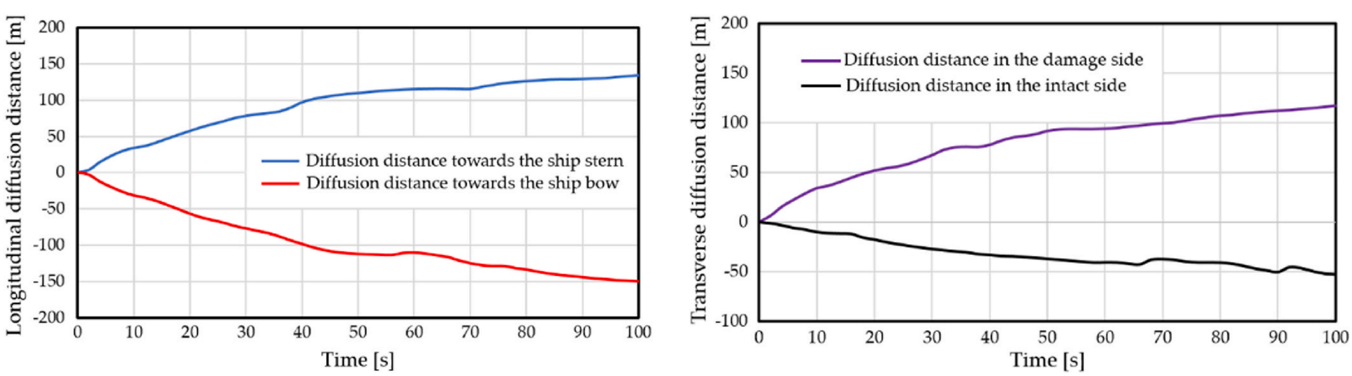

Fig. 13. Diffusion distance of RPT gas in beam wind towards the damaged side of LNG carrier.

leakage process of the cryogenic LNG and considering the influence of different wind directions. The main contents are summarized as follows. Section 2 describes the applied damaged model, including the main particulars and damage details. Section 3 introduces numerical scheme and settings, including the initial distribution of multiple fluids based on User Defined Function (UDF) and typical numerical settings. Section 4 performs the numerical convergence analysis in the no-wind scenario (Case 0), including the mesh and time-step sensitivity analysis. Section 5 further discusses numerical results of four leakage scenarios, including the beam wind scenario towards the damaged side of the damaged LNG carrier (Case 1), the beam wind scenario towards the intact side of the damaged LNG carrier (Case 2), the head wind scenario towards the bow of the damaged LNG carrier (Case 3) and the following wind scenario towards the stern of the damaged LNG carrier (Case 4). To further clarify the influence of external wind, Section 6 performs the comparison analysis between the no wind and wind scenarios. Finally, main conclusions are detailed in Section 7.

2. Description of the damaged ship

Fig. 2 presents the damaged model used in this paper, which is a typical Moss-B spherical tank LNG carrier. This ship has five independent, self-supporting cargo tanks with the damage opening set on the starboard side of NO. 3 tank. To simplify the simulation, a circular opening with a diameter of 1.6 m is adopted, and the model only includes the main hull, excluding the superstructures. According to the loading manual, the full load condition is used as the test condition for this study. Table 1 shows the ship's information and details of the damage opening. The numerical simulation will not include the motion response of the damaged vessel, so there is no need to determine the specified center of gravity and moment of inertia.

Based on the ship model described above, five simulation cases were performed as shown in Fig. 3, including the no-wind scenario (Case 0), the beam wind towards the damaged side (Case 1), the beam wind towards the intact side (Case 2), the head wind (Case 3) and the following

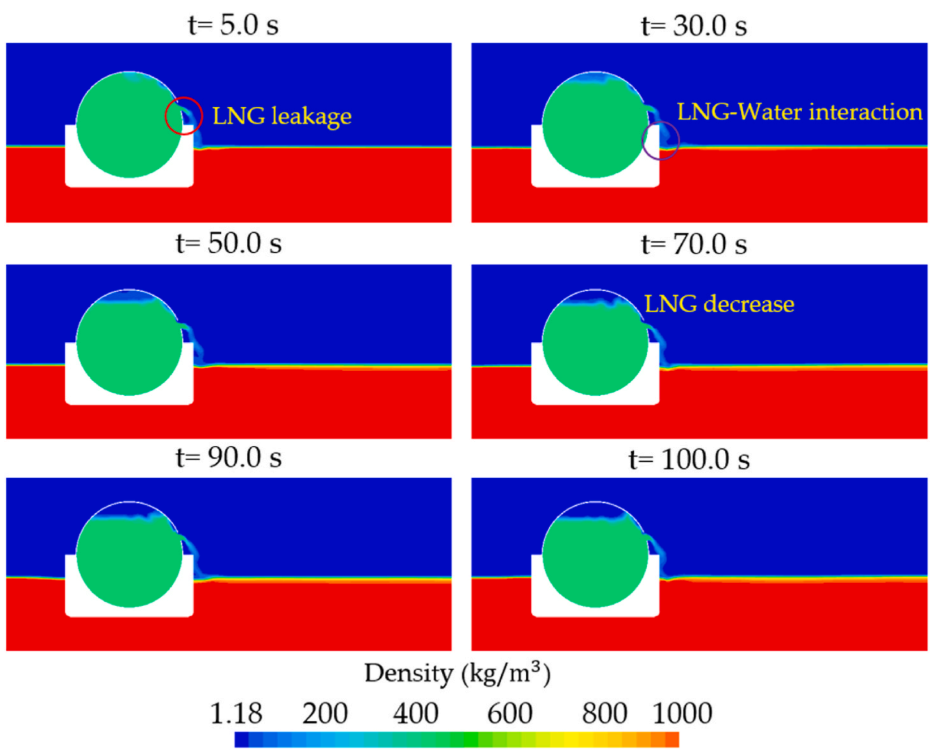

Fig. 14. Dynamic leakage process in the beam wind towards the intact side of LNG carrier.

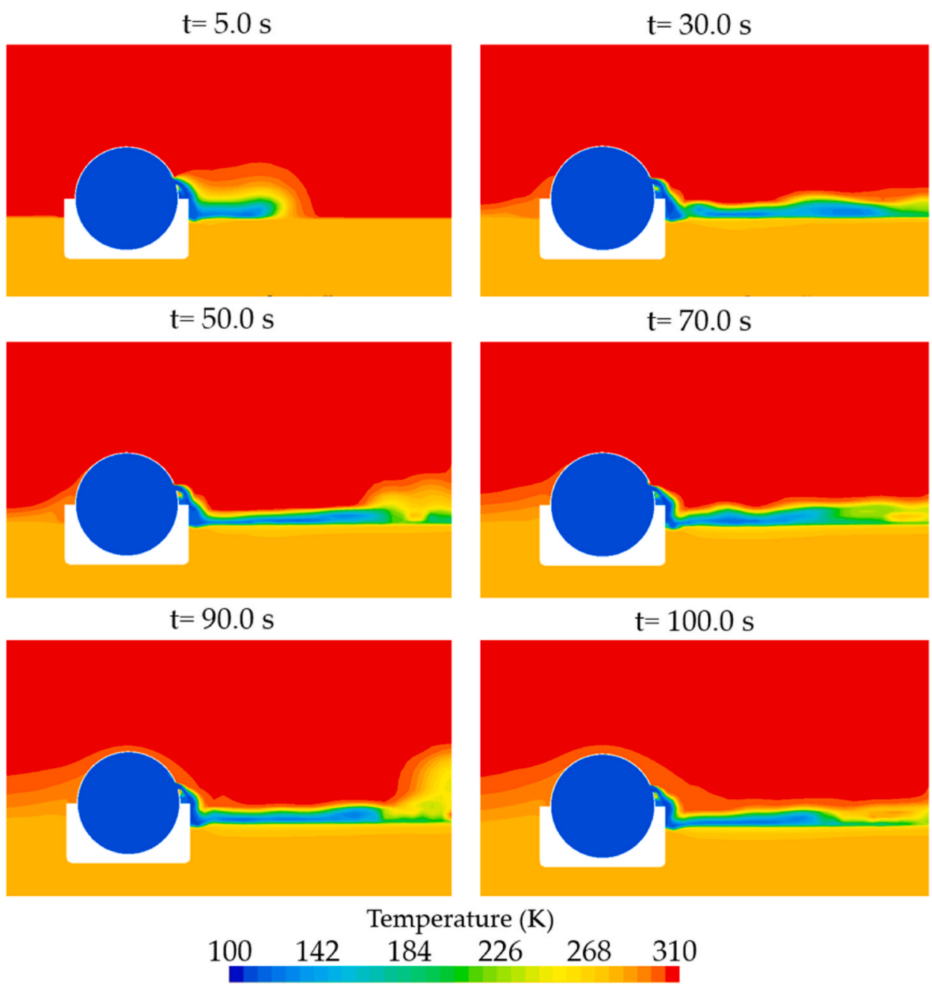

Fig. 15. Temperature field in the beam wind towards the intact side of LNG carrier.

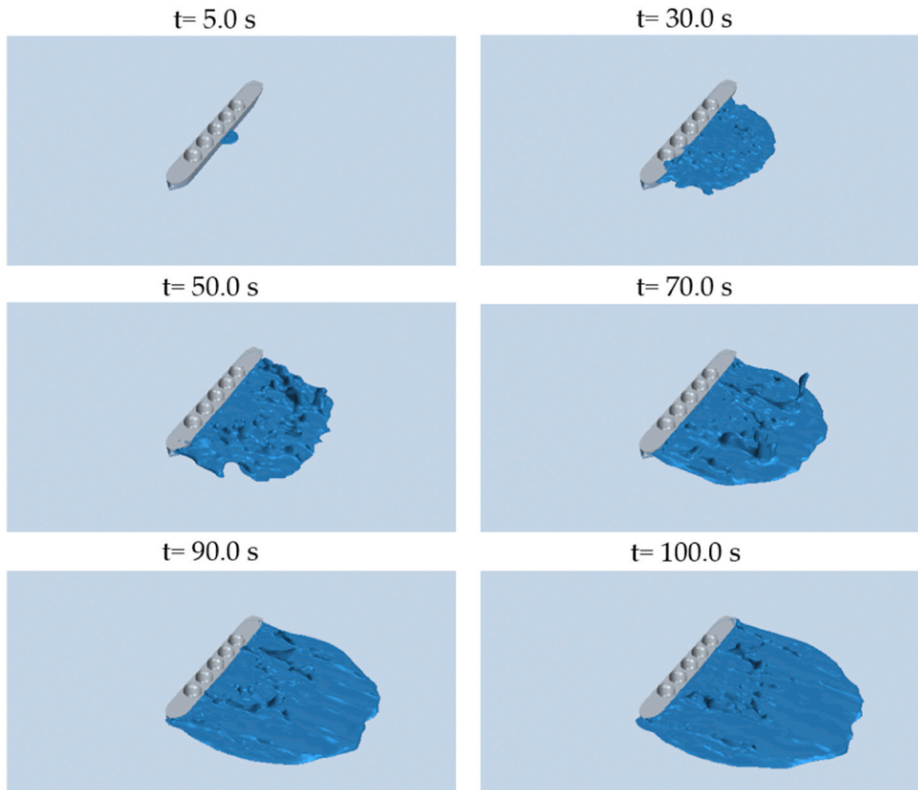

Fig. 16. Diffusion behavior of RPT gas in the beam wind towards the intact side of LNG carrier.

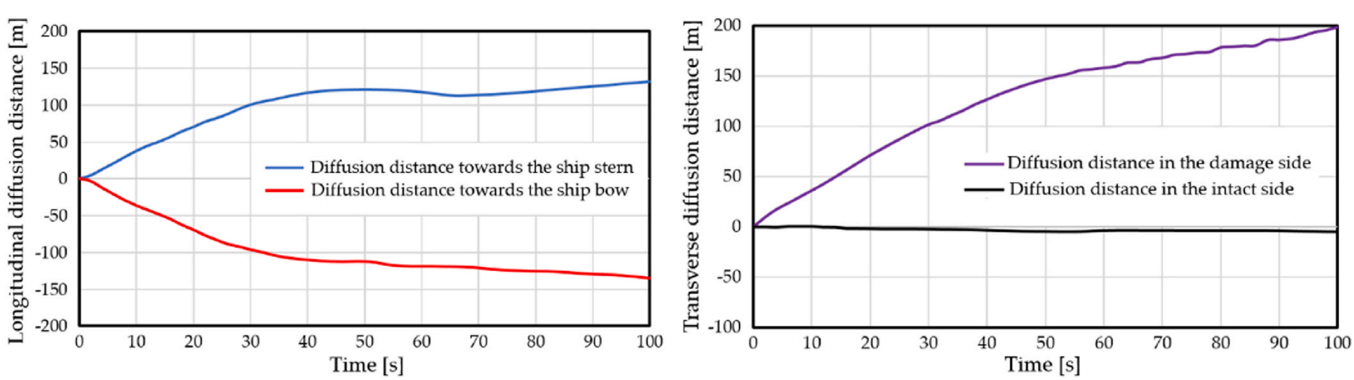

Fig. 17. Diffusion distance of RPT gas in in beam wind towards the intact side of LNG carrier.

wind (Case 4). The no-wind case is used to perform numerical convergence analysis in Section 4. The other four cases are used to analyze RPT and diffusion characteristics, as described in Section 5.

3. Numerical simulation settings and setup

The present work extends that of Zhang et al. (2025). The applied numerical simulation method is composed of two modules, including the CFD module and the boiling module in the multiphase interaction model. In the CFD module, the multiphase model is used to define multiphase fluids. To determine the turbulent eddy viscosity and govern the mean flow quantities, the K-Epsilon turbulence model is applied to solve transport equations for the turbulent kinetic energy and the turbulent dissipation rate.

Considering the mixing flow of several immiscible fluids, the VOF method with the High-Resolution Interface Capture (HRIC) scheme is used to resolve the position and shape of the interface between phases. The implicit unsteady model with the segregated flow model controls the iteration step and time step. Furthermore, the Cell Quality Remediation model is used to modify poor-quality cells to improve the robustness of the numerical solution. Finally, a UDF (User-Defined Function) based on the Cell_Set operation enables the initial distribution of multiphase fluids.

In the boiling module, the RPT mechanism is controlled by the multiphase material model, the Rohsenow model, and VOF boiling models. The interphase interaction model is also utilized to control the primary and secondary phases in the RPT process. Generally, during phase transition, when the primary phase contacts with another fluid phase, and the temperature of the latter is higher than the saturation temperature of the former, the primary phase will be transformed into a secondary phase. Furthermore, differently from the no-wind condition in Zhang et al. (2025), in the present study it is considered a wind speed of 4.0 m/s using the VOF wave model.

The next section specially explains how to use the Cell_Set operation

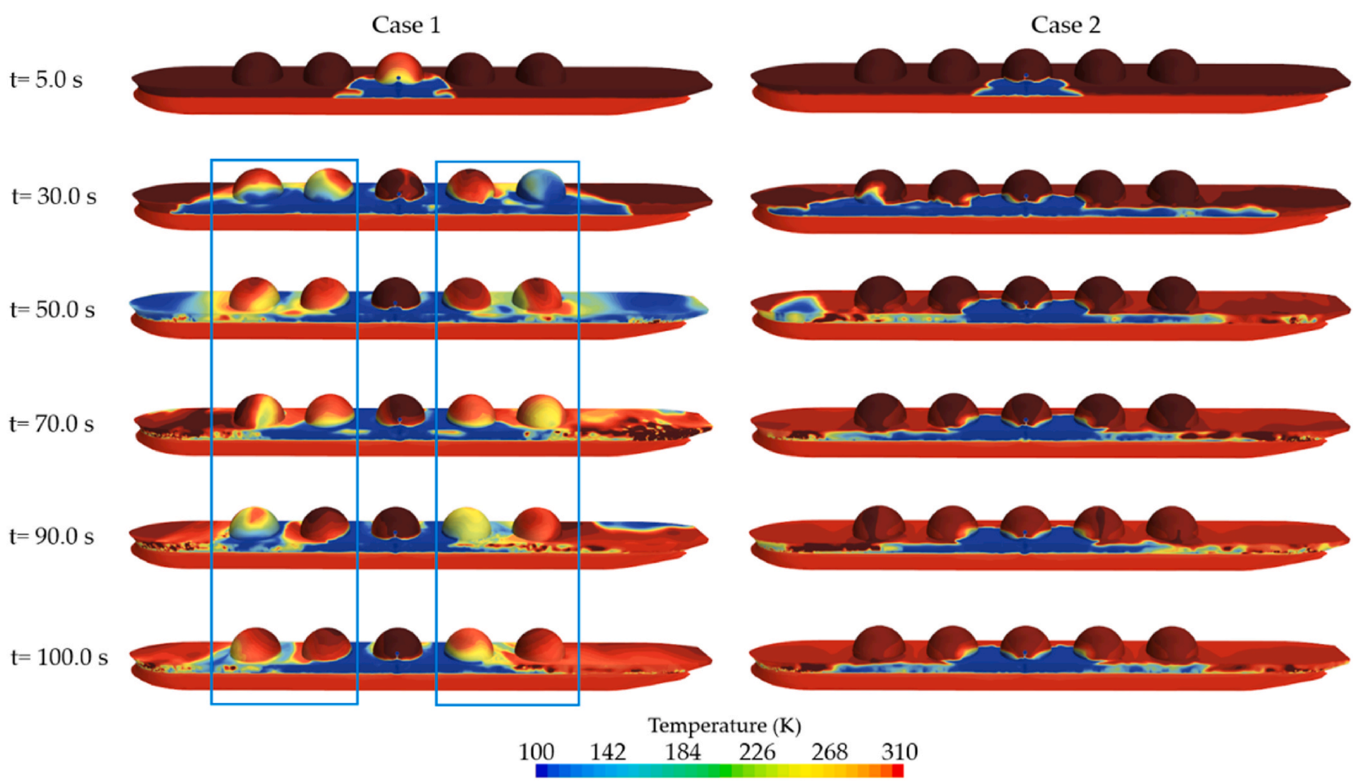

Fig. 18. Temperature comparison on the hull surface between Case 1 and Case 2.

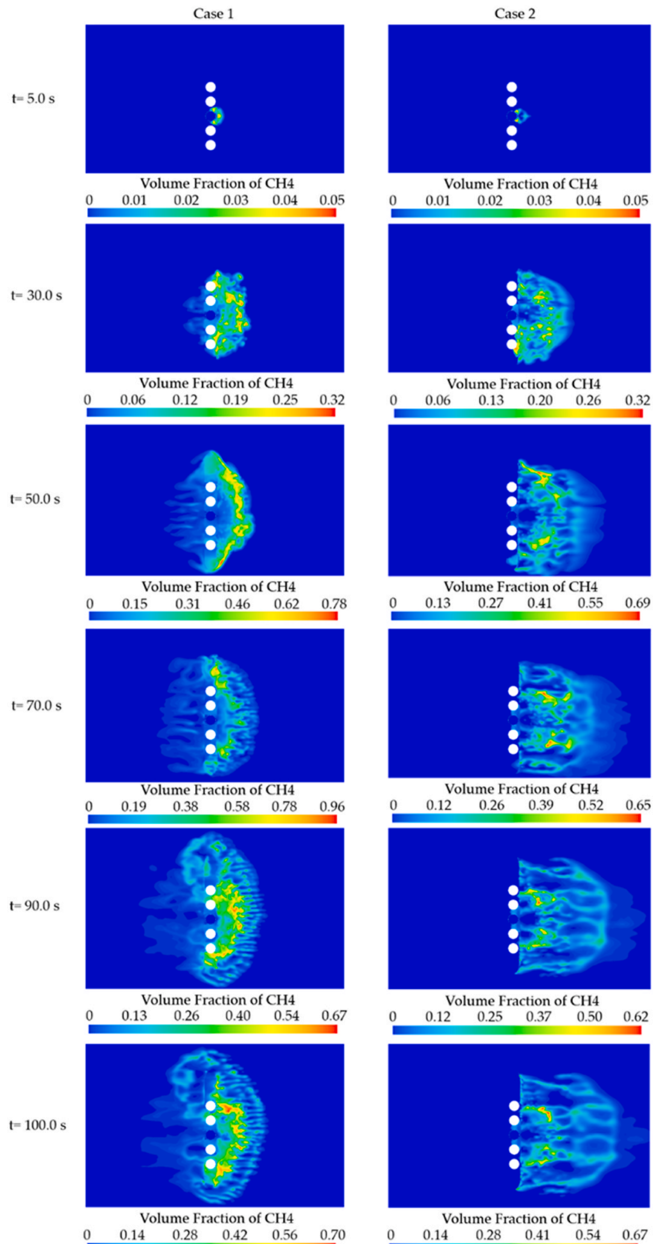

Fig. 19. Concentration comparison of CH4 between Case 1 and Case 2.

to distribute the region. Finally, this section will discuss the simulation domain and the mesh generation process.

3.1. *Initial distribution of multiphase fluids based on UDF function*

Different from the conventional hydrodynamic calculation involving only two phases (gas-liquid), leakage simulation of the cryogenic LNG requires the coupling of multiphase fluids, including water, air, LNG and the phase-transition gas. As shown in Fig. 4, in addition to water and air in the external environment, the cryogenic LNG in its initial state is stored in the cargo tank. When damage occurs, the cryogenic LNG leaks from the cargo tank, and RPT behavior occurs when it comes into contact with air and water. Considering the challenge of multi-component liquids and gases to simulation efficiency, single-component methane is used to simplify the LNG and phase-transition gas. Table 2 displays the physical properties of the different fluids. It is worth noting that to reflect the effects of gas-liquid interaction on leakage and diffusion, the compressibility characteristic of air and the phase-transition gas is taken into consideration by the ideal gas model.

To realize the initial distribution of the multiphase fluids in Fig. 4 and define physical properties in Table 2, the numerical simulation in this paper needs to apply UDF function and Cell_Set operation. As shown in Fig. 5, except for the empty region inside the hull, the remaining simulation domain is divided into four regions through Cell_Set operation. The following content will explain the role of the regional division in combination with the specific form of UDF function.

Equations (1)–(3) respectively present the UDF functions corresponding to the initial distribution of different fluids. Equation (1) represents the compartment space of LNG cargo tank by combining Region 1 and Region 2. Equation (2) represents the space where water is located through the difference between the space below the waterline and Region 1. Equation (3) represents the space where air is located through the difference between the space above the waterline and Region 2. It is worth noting that $$Position [2] represents the position of the free surface, which needs to be set according to the draft under the full load in Table 1. In general, the principle of the region division is that

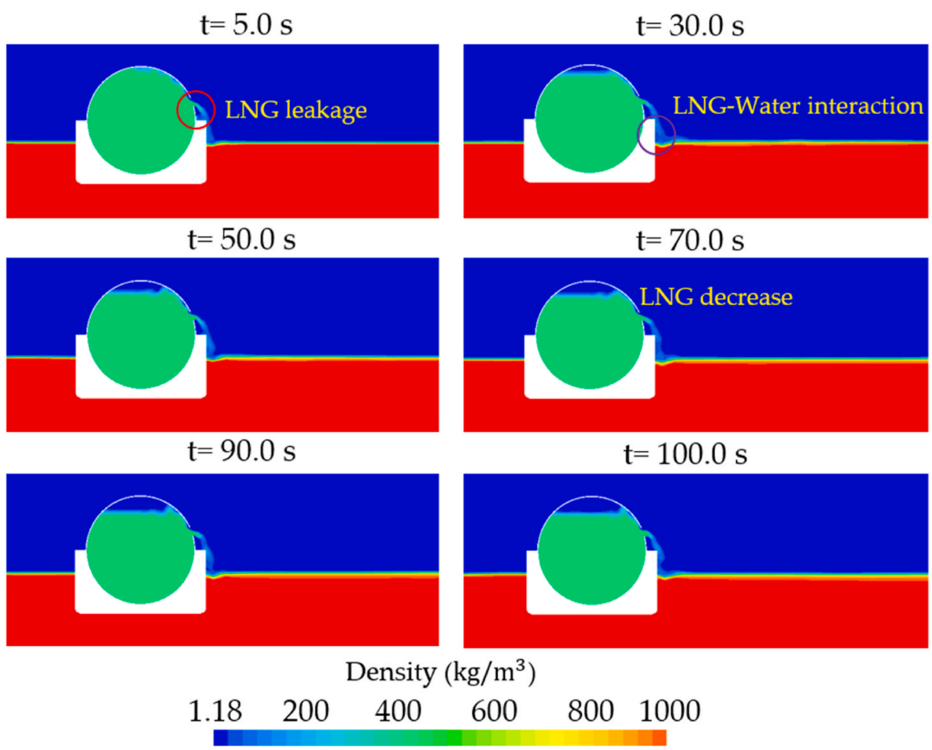

Fig. 20. Dynamic leakage process in the head wind towards the ship stern of LNG carrier.

only one fluid phase can exist in one region space. Moreover, the UDF form must strictly follow the software language to avoid error reports.

$$(\text{Region [1] + Region [2]})?\ 1{:}\ 0 \tag{1}$$

$$(\$\$\text{Position [2]} \leq 7.6\text{-Region [1]})?\ 1{:}\ 0 \tag{2}$$

$$(\$\$\text{Position [2]} \geq 7.6\text{-Region [2]})?\ 1{:}\ 0 \tag{3}$$

After resolving the initial distribution of different fluid phases, the density and dynamic viscosity of the fluid phase in Table 2 can be specified accordingly through the multiphase model. However, the temperature in Table 2 still needs to be defined with a UDF function. Equations (4)–(6) respectively present the forms of the UDF functions defining the temperatures of different fluid phases. The temperatures of water, air and LNG are set to 278 K, 306 K and 111 K.

$$(\text{Region [1] + Region [2]})?\ 111{:}\ 0 \tag{4}$$

$$(\$\$\text{Position [2]} \leq 7.6\text{-Region [1]})?\ 278{:}\ 0 \tag{5}$$

$$(\$\$\text{Position [2]} \geq 7.6\text{-Region [2]})?\ 306{:}\ 0 \tag{6}$$

3.2. Simulation domain and mesh generation

The numerical simulation in this paper assumes that the damaged LNG carrier is stationary. In this case, the mesh discretization in a single background region is sufficient to solve the physical problems involved in the leakage process.

As shown in Fig. 6, the above-water part of the LNG carrier is placed in the simulation domain, and the simulation domain should have enough space to ensure the full propagation of the wind field on both sides of the LNG carrier. Moreover, an appropriate boundary condition will also guarantee the accuracy of the numerical results. Taking the head wind on the LNG carrier as an example, Table 3 presents the boundary conditions. The outlet boundary in Fig. 6 is set as the pressure outlet, and the inlet, top and bottom boundaries are set as the velocity inlet. Hidden sides are set as the symmetry plane to realize an infinite space. The principle of setting the boundary condition is that a pressure outlet should be set at the wind outlet to simulate the leakage scenario in the natural environment.

Regarding the mesh generation shown in Fig. 7, specific controls have been applied to capture the behavior of the leakage process, as follows:

- The mesh near the damaged cargo tank needs to be locally refined.
- To better reflect the influence of the wind field on the hull, the mesh near the free surface in the direction of the wind propagation needs to be locally refined.
- Considering the complex curvature of the hull surface, the mesh generation should ensure the actual shape of the hull surface while minimizing grid resultion to improve the simulation efficiency. As for the mesh generation in other leakage scenarios, it can be carried out in accordance with the above guidelines.

4. Numerical convergence analysis

4.1. Mesh sensitivity analysis

To achieve the balance between the mesh number and the mesh accuracy, a specific study was first carried out to analyze the mesh sensitivity for the no-wind case. As shown in Fig. 8, according to the ITTC Procedures and Guidelines: Practical Guidelines for Ship CFD Applications (2011), three mesh scenarios were obtained by adjusting the local size of the grid, with the number of cells being 1116060, 2585988, and 5553388 respectively. It is worth noting that a constant time-step of 0.0025s is kept for all these cases. The key parameter for the mesh sensitivity analysis was identified as the maximum horizontal diffusion range of a 15 % concentration of methane at 5 s after the leakage.

Fig. 8 (a) compares the maximum diffusion range in three mesh scenarios, which are 34.385 m, 34.784 m and 34.791 m. From Fig. 8 (b), it can be seen that a monotonic convergence is detected and when

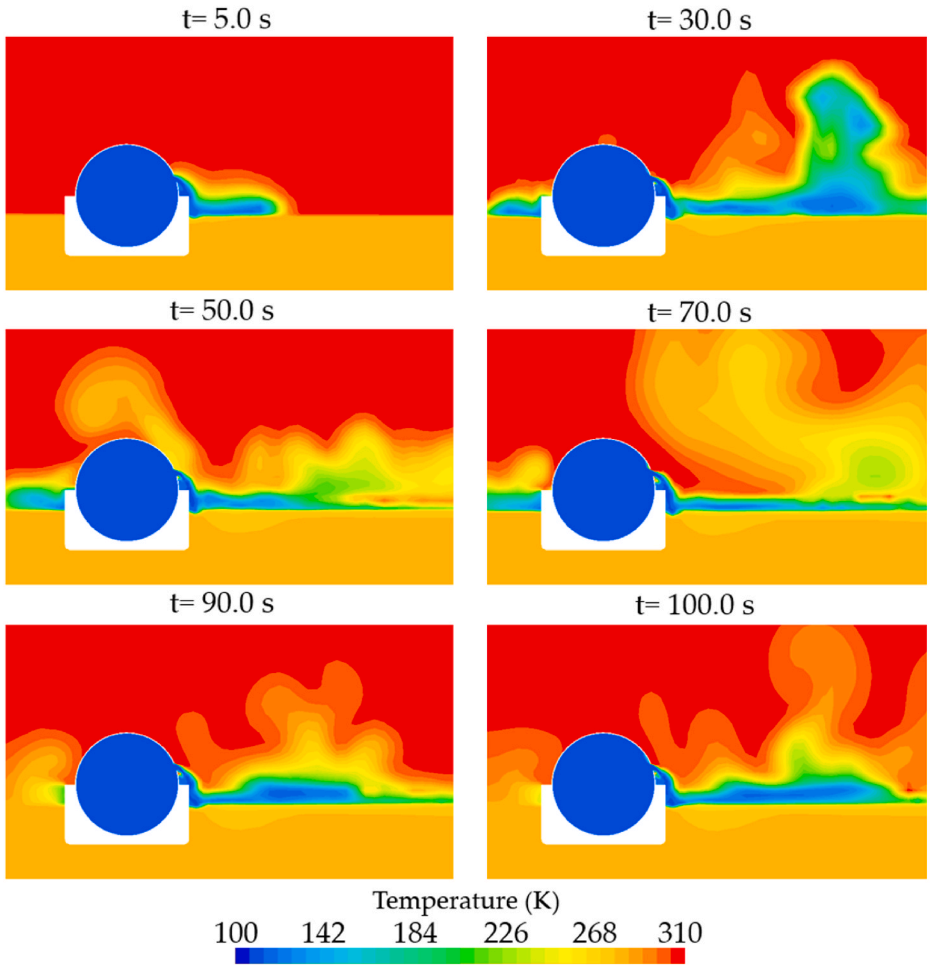

Fig. 21. Temperature field in the head wind towards the ship stern of LNG carrier.

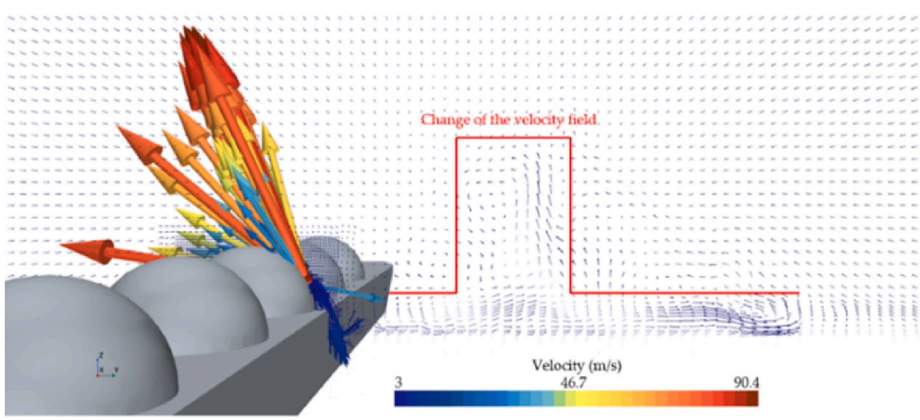

Fig. 22. Details of the velocity filed at the typical 30 s moment in Case 3.

compared to the coarse and fine mesh scenarios, the medium mesh ensures a good compromise between the result convergence and computational effort. In Fig. 8 (b), h_i/h_1 represents the ratio of cells between the specific mesh case and the coarse one.

4.2. Time-step sensitivity analysis

A time-step sensitivity analysis was conducted using the medium mesh case described in Section 4.1. Similar to the mesh sensitivity analysis, Fig. 9 (a) compares the maximum diffusion range in three different time step cases. A time-step of 0.0025 s can better reflect the intensity of phase transition gas diffusion. Fig. 9 (b) shows that even for the time-step sensitivity analysis a monotonic convergence is detected and the numerical results achieved with a time-step of 0.0025 s can be considered as a good balance between computational efforts and accuracy of the simulation results.

5. Numerical results in different wind scenarios

This section will introduce the numerical results in different wind

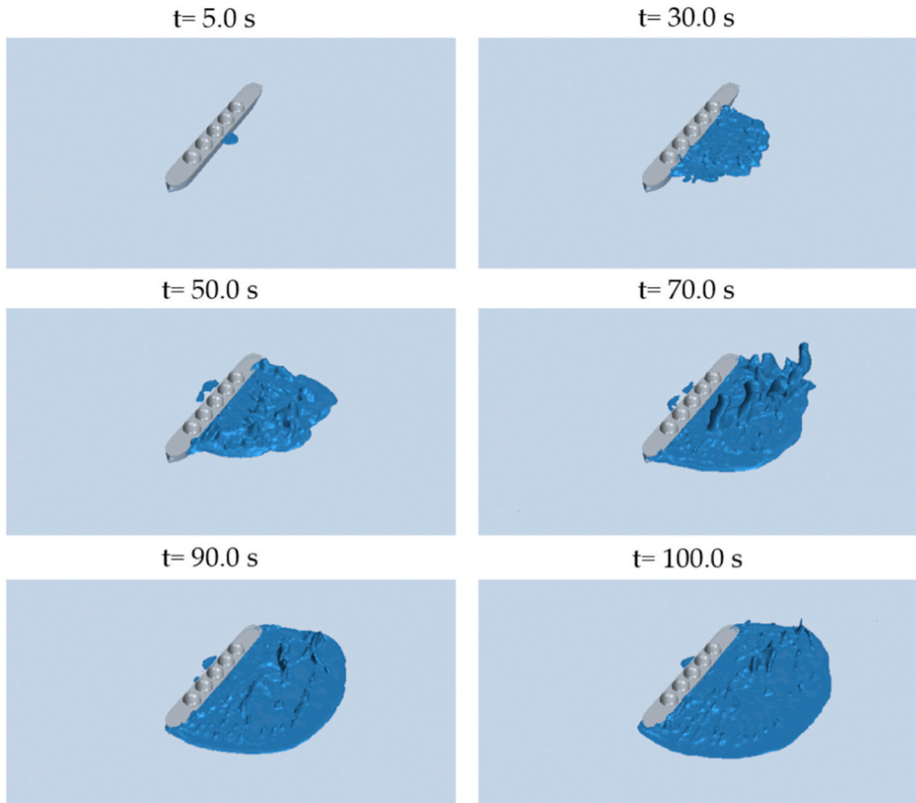

Fig. 23. Diffusion behavior of RPT gas in the head wind towards the ship stern of LNG carrier.

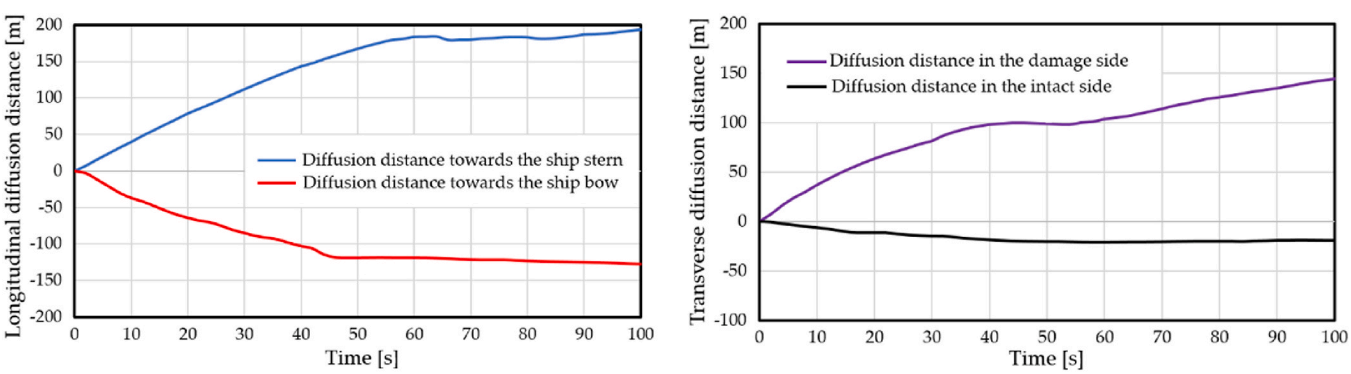

Fig. 24. Diffusion distance of RPT gas in the head wind towards the ship stern of LNG carrier.

scenarios, including the leakage process in the density field, the spatial distribution of the cryogenic environment in the temperature field, the diffusion behavior of the phase-transition gas in the 5 % concentration methane scenario, the concentration distribution of the methane in the volume fraction scenario, and the influencing range of the cryogenic environment on the hull surface in the temperature field. The purpose of the numerical analysis can be divided into the following two aspects.

(1) By visualizing microscopic hydrodynamic behavior, a better understanding of the RPT characteristics can be achieved.
(2) By comparing the numerical results in different wind scenarios, the influence of the wind direction on the cryogenic diffusion and methane concentration can be explored. The research results can provide valuable references for the explosion prevention, optimization design of the hull structure, and leakage emergency management.

5.1. *Case 1: Beam wind towards the damaged side of LNG carrier*

Fig. 10 presents the dynamic leakage process of the cryogenic LNG in the beam wind towards the damaged side of the LNG carrier. It can be observed that at the moment of leakage, the LNG in the cargo tank will gradually leak from the damaged opening due to gravity. The leaked LNG will first encounter the ship deck and then flow into the seawater. As shown in the leakage process at 30 s in Fig. 10, the behavior of LNG interacting with the deck and water can be clearly seen. As the leakage progresses, the amount of LNG in the cargo tank gradually decreases, as shown in the leakage process at 70 s in Fig. 10. Since a small damaged opening was applied in this paper, even after 100 s, as shown in Fig. 10, the leakage process continues.

The LNG leakage will have a significant effect on the temperature field near the hull. Fig. 11 shows the temperature field at the same timing as Fig. 10, which has the following characteristics:

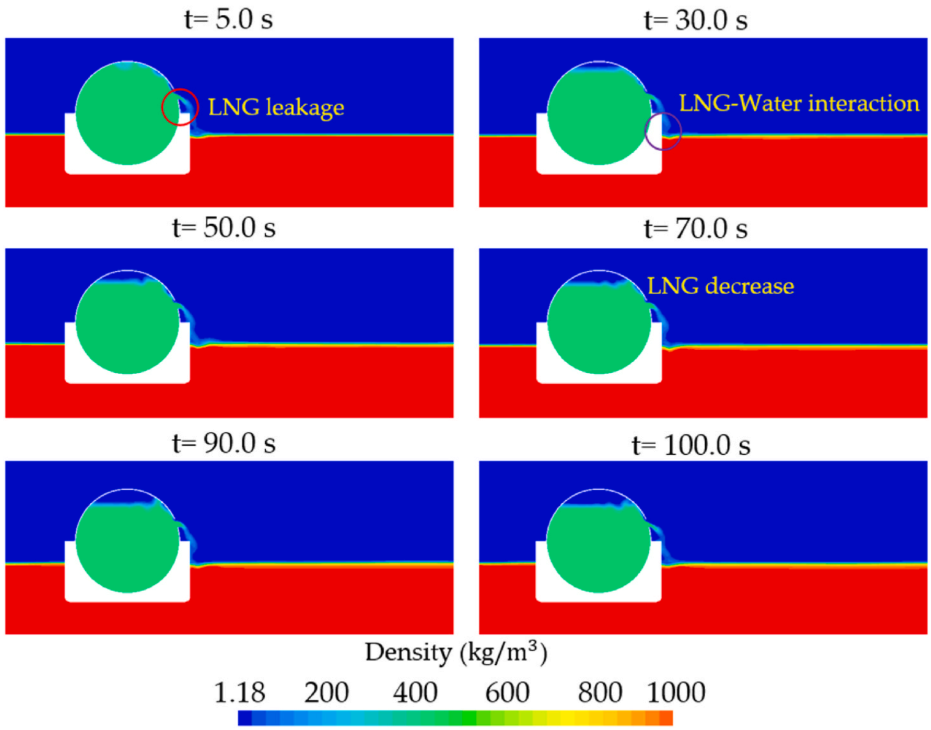

Fig. 25. Dynamic leakage process in the following wind towards the ship bow of LNG carrier.

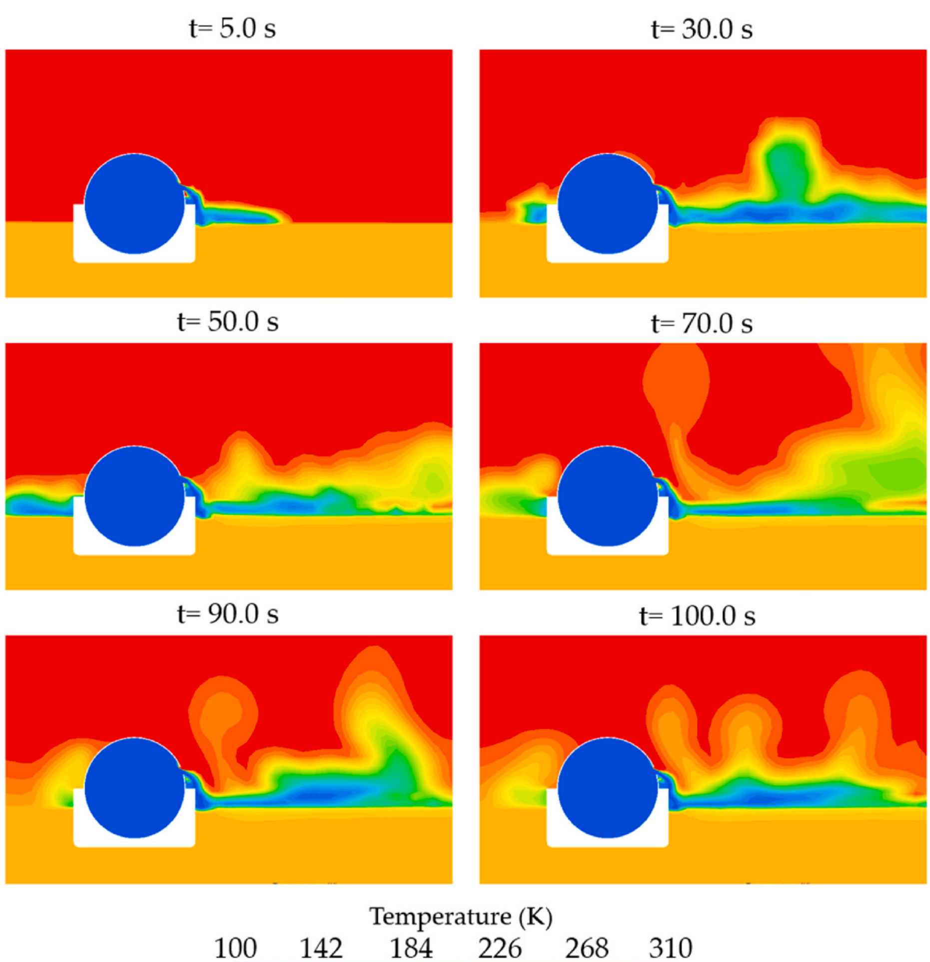

Fig. 26. Temperature field in the following wind towards the ship bow of LNG carrier.

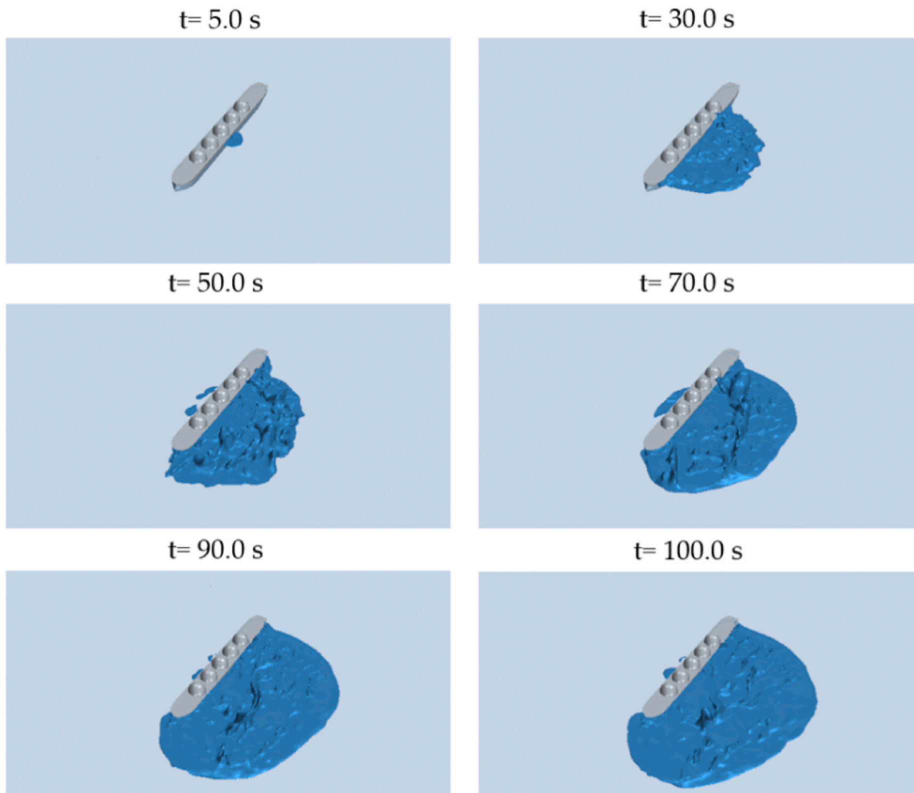

Fig. 27. Diffusion behavior of RPT gas in the following wind towards the ship bow of LNG carrier.

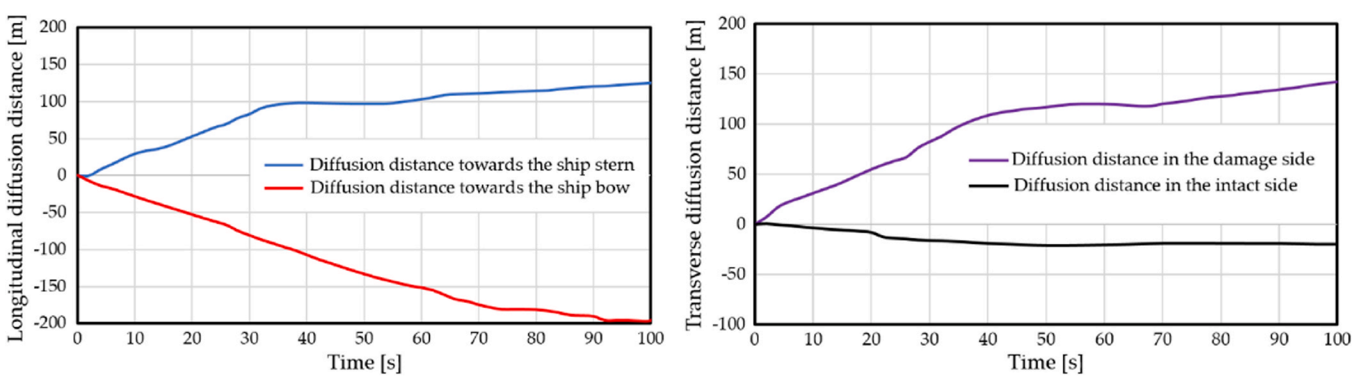

Fig. 28. Diffusion distance of RPT gas in the following wind towards the ship bow of LNG carrier.

- First, most of the leaked LNG is concentrated on the damaged side, and the cryogenic environment will also be distributed on the damaged side.
- Second, the leaked LNG will interfere with the deck, and the cryogenic environment will spread through the deck to the intact side of the damaged LNG carrier. As shown in the temperature field at 50 s in Fig. 11, the cryogenic environment is observed on both sides of the LNG carrier.
- Third, since the leakage direction of LNG is opposite to the wind direction, even if the density of the cryogenic phase-transition gas is greater than that of air, the continuous beam wind will bring more of the cryogenic environment to the intact side of the LNG carrier. As shown in the temperature details at 30 s, 50 s, 70 s, 90 s and 100 s in Fig. 11, the beam wind towards the damaged side of the LNG carrier intensified the spatial variation of the temperature field.

With the aim of explaining the temperature details in Figs. 11 and 12 displays the diffusion behavior of the phase-transition gas during the leakage process through the methane concentration field. It can be found that under the influence of the beam wind towards the damaged side of LNG carrier, the cryogenic phase-transition gas will bypass the damaged hull and diffuse in the intact side. Combining the temperature fields at 30 s and 50 s in Fig. 12, it can be clearly found that there is RPT gas in the cryogenic space on the intact side. Especially for the temperature field at 70 s in Fig. 11, the temperature change above the cargo tank is caused by the cryogenic phase-transition gas floating above the hull deck. To sum up, when the damaged LNG carrier is in the beam wind towards the damaged side of the LNG carrier, both sides and the upper space of the vessel will be affected by the cryogenic environment.

In this case, the damaged LNG carrier will encounter the greatest disaster risk. To more specifically demonstrate the extent of the cryogenic environment's influence, Fig. 13 presents the time-history curves of the diffusion range of the phase-transition gas in four directions of the LNG carrier. It can be found that since the damage opening on the NO.3

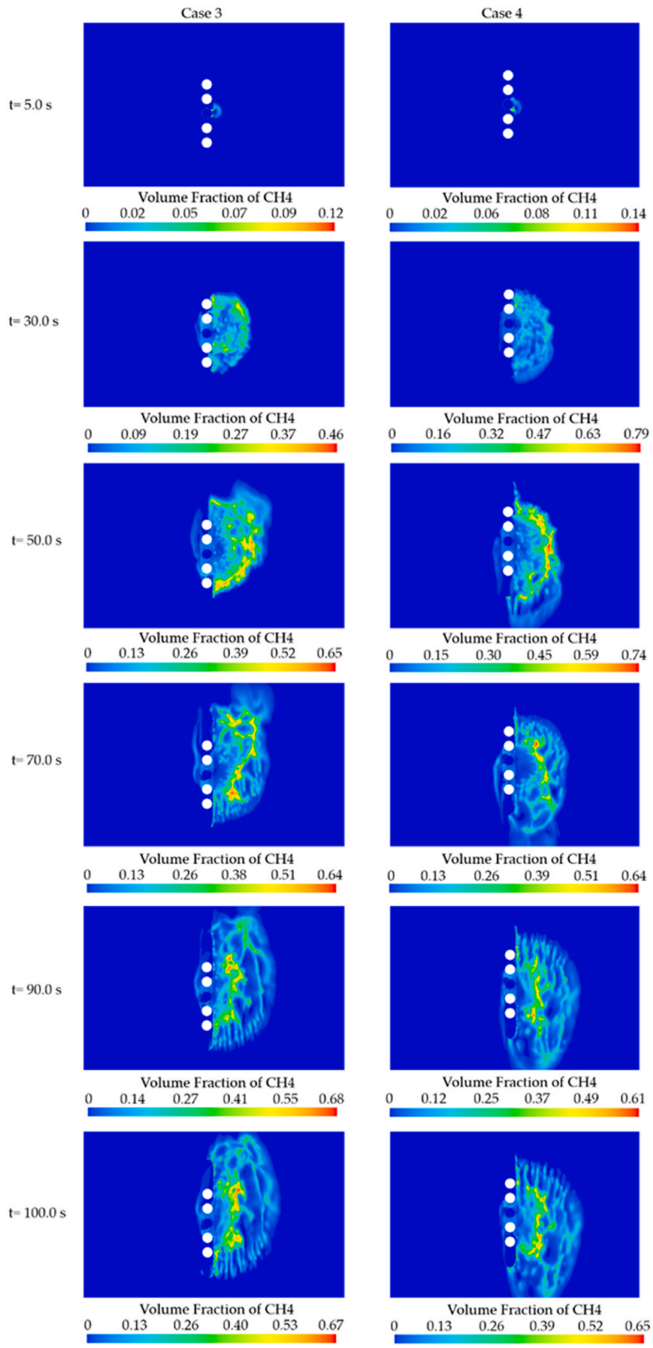

Fig. 29. Concentration comparison of CH4 between Case 3 and Case 4.

cargo tank is located near the middle of the LNG carrier, the propagation of the phase-transition gas in the bow and stern directions is basically symmetric. Judging from the range on both sides in Fig. 13, the diffusion range of the phase-transition gas on the damage side is much greater than that on the intact side. From the specified diffusion range at 100 s after the leakage occurred, the diffusion distance of the phase-transition gas on the intact side is 50 m while the diffusion distance of the phase-transition gas on the damage side can reach 120 m. The results from multiple perspectives can provide an understanding of the leakage characteristics.

5.2. *Case 2: Beam wind towards the intact side of LNG carrier*

As shown in Fig. 14, the dynamic leakage process of LNG in the beam wind towards the intact side of the LNG carrier is presented. Comparing with the leakage process in Fig. 10, it can be observed that the direction of the beam wind does not have a significant effect on the overall leakage process. The leakage process is also accompanied by the dynamic details, including the LNG leakage at the damage opening and the LNG-Water interaction behavior on the free surface. The decrease in LNG levels after 100 s in both beam wind scenarios is also similar. This is primarily because the cargo tank is a closed space, in which the narrow opening and the RPT behavior will prevent air from entering the damaged tank, neither accelerating nor delaying the leakage process.

Although different directions of the beam wind did not have a significant effect on the leakage process, the temperature fields and the spatial distribution of the phase-transition gas in different scenarios deserve further analysis. As shown in Fig. 16, the beam wind towards the intact side of the damaged LNG carrier will push the leaked LNG to continuously spread on the damaged side and alleviate the diffusion in the height direction. The cryogenic environment only affected the damaged side of the LNG carrier, while the intact side remained at the original temperature condition. Moreover, as shown in the temperature field at 90 s and 100 s in Fig. 15, the flowing wind will affect the temperature field near the free surface. After interfering with the LNG carrier, a phenomenon of the path line will form on the surface of the cargo tank.

To better explain the temperature distribution represented in Figs. 15 and 16 shows the diffusion behavior of the phase-transition gas towards the intact side in three-dimensions. The beam wind in the same direction as the damaged leak effectively prevents the cryogenic phase-transition gas from affecting the hull structure.

Fig. 17 shows the diffusion distance of the phase-transition gas in different directions of the hull. Like Fig. 13, the phase-transition gas is symmetrically distributed in the bow and stern directions. However, since the direction of the beam wind is **in the same direction as** the leak, coupled with the hindering effect of the hull, the phase-transition gas does not spread to the intact side of the damaged LNG carrier. Therefore, when the damaged LNG carrier takes wind from the beam side, the beam wind in the same direction as the damaged side is more conducive to ensuring the safety of the hull structure.

When considering the influence of the cryogenic environment on the hull structure, Fig. 18 compares the temperature distribution on the hull surface in two beam wind scenarios. For the hull surface in the damage side of the LNG carrier, five cargo tanks were all affected by the cryogenic environment at different times. Moreover, not only were the surfaces of the cargo tanks affected, but also the hull deck, with the impact extending to the bow and stern. However, in the beam wind towards the intact side scenario, except for the tanks close to the NO.3 tank, the other tanks and adjacent hull surface are not in the cryogenic environment for a long time. Therefore, in terms of the safety of the hull structure, the beam wind towards the intact side of the LNG carrier can greatly alleviate the brittle damage of the hull surface by the cryogenic environment.

In addition to the influence of the cryogenic environment on the hull structure mentioned above, the methane concentration in the leakage process will also determine whether there is an explosion risk in the rescue management. Fig. 19 compares the methane concentration near the free surface in Case 1 and Case 2 at the same leakage points. The numerical results for Case 1 reveal that, due to the hindering effect of the hull, the phase-transition gas was mostly concentrated near the LNG carrier. Conversely, the phase-transition gas in Case 2 was blown away by the wind, and the beam wind played a diluting role. The maximum volume fraction of methane during Case 1 is greater than that in Case 2. As shown in the volume fraction values for Case 1 and Case 2 in Fig. 19, the maximum value for Case 1 is 0.96 while the maximum value for Case 2 is 0.65.

Moreover, the highest methane concentration in Case 1 is closer to the hull due to the crosswinds in different directions. This means that the leaking methane is more likely to explode currently, putting the hull

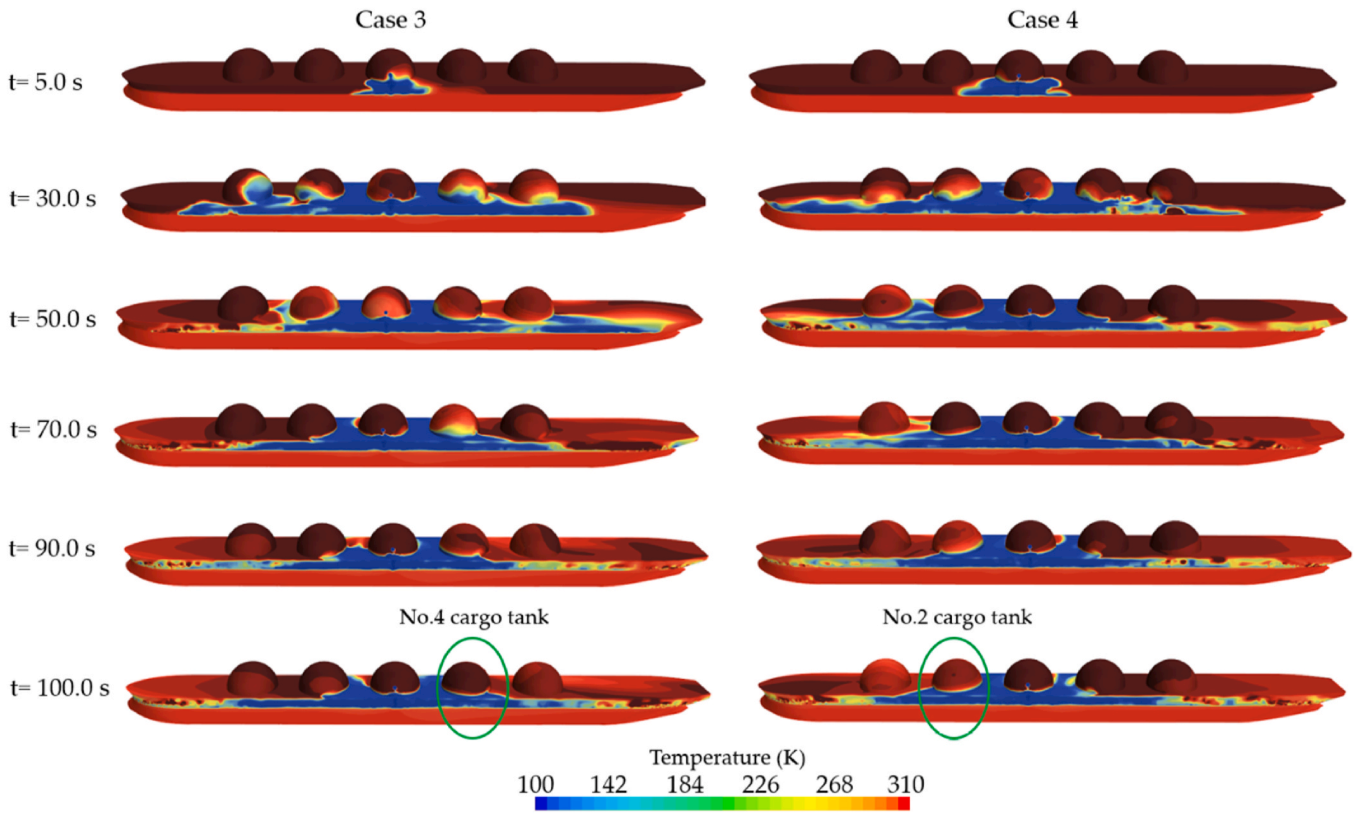

Fig. 30. Temperature comparison on the hull surface between the head and following wind scenarios.

structure at greater risk of damage. Overall, no matter from the perspective of brittle damage caused by the cryogenic environment or explosion risk, the beam wind towards the intact side of the LNG carrier in Case 2 can effectively alleviate the threat. Obtained results can provide references for the rescue and loss prevention of the damaged LNG carriers.

5.3. *Case 3: Head wind towards the ship stern of LNG carrier*

Considering that the wind direction is always changing, the LNG carrier will encounter two wind scenarios, including the head wind and the following wind. It is also of great significance to study the leakage process and diffusion of the damaged LNG carrier in these two scenarios.

Fig. 20 shows the dynamic leakage process of the damaged LNG carrier in the head wind condition. By comparing it with the density fields in the beam wind scenarios of Section 5.1 and Section 5.2, it can be found that the head wind has no significant effect on the leakage process. Fig. 21 shows details of the temperature field at the same moments as Fig. 20. Like Fig. 11, the head wind will also cause both sides of the damaged LNG carrier to be affected by the cryogenic environment. As shown in the temperature field at 30 s and 70 s in Fig. 21, the cryogenic dispersion range above the free surface is wider, indicating that the head wind will intensify the change of the temperature field on the damage side. To microscopically display the characteristics of the flow field in the dispersion space, Fig. 22 shows the vector of the velocity field at 30 s. It can be found that the velocity vector nonlinearly points different directions. Moreover, it can be found that the rapid phase transition of the cryogenic LNG is extremely intense accompanied by a phase-transition gas velocity of 90 m/s near the damage opening. This may have a huge effect on the adjacent hull structures of the damaged LNG carrier.

To explain the causes of the cryogenic environment in Figs. 21 and 23 shows the diffusion behavior of the cryogenic phase-transition gas. Like Fig. 12, the head wind towards the ship stern causes part of the cryogenic phase-transition gas to spread to the intact side of the ship, which explains the reason for the cryogenic environment occurring on both sides of the LNG carrier in Fig. 21. Moreover, combined with the hydrodynamic details of Figs. 21 and 23 in the 70 s, the upward diffusion of the phase-transition gas causes the temperature to descend. Fig. 24 shows the diffusion distance of the phase-transition gas in different directions of the hull. The head wind makes the phase-transition gas spread over a large area in a stern direction. Although the gas in the head wind can also spread on the intact side of the LNG carrier, due to the obstruction of the hull, it only diffuses within a limited area. As shown in Fig. 24, until 100 s after the leakage occurs, the diffusion distance of the phase-transition gas on the intact side is approximately 15 m.

5.4. *Case 4: Following wind towards the ship bow of LNG carrier*

Contrary to the direction of the head wind in Section 5.3, Figs. 25–28 respectively show the density field, temperature field, diffusion behavior of the phase-transition gas and diffusion distance of the phase-transition gas in the following wind. These visualized microscopic hydrodynamic details have been explained in Sections 5.1, 5.2 and 5.3.

Fig. 29 compares the methane concentrations in the head and following wind scenarios. It is noticeable that the concentration and distribution of the phase-transition gas are affected by the wind direction, and the following aspects can be highlighted:

1) For both head and following wind scenario, the wind will cause most of the phase-transition gas to be concentrated in the downwind area.
2) Like Case 2 where the beam wind points to the intact side of the damaged LNG carrier, the head and following wind also cause the phase-transition gas to spread mainly on the damaged side of the LNG carrier.
3) Different from the comparison results in Fig. 19, the head and following wind do not have a significant effect on the methane concentration in Case 3 and Case 4 of Fig. 29. The subtle difference is

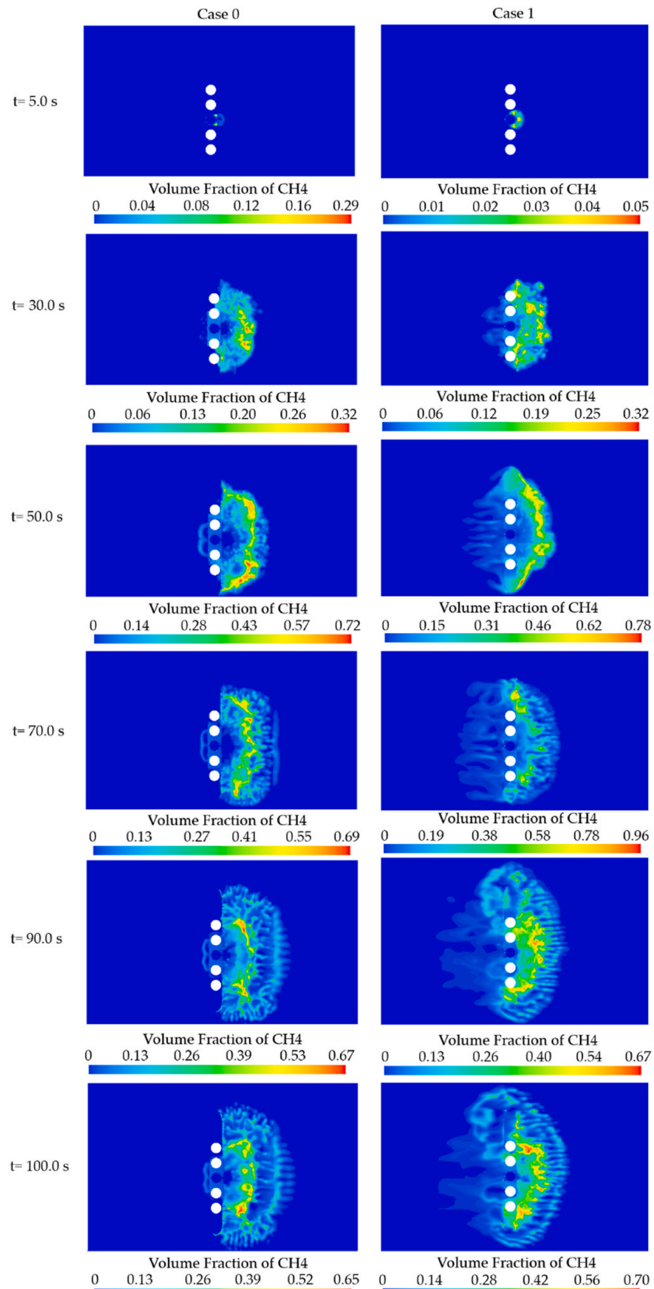

Fig. 31. Concentration comparison of CH4 between Case 0 and Case 1.

due to the different shapes of the ship's bow and stern, which will subsequently affect the velocity fields near the hull ends.

Overall, based on the spatial distribution of the cryogenic environment, the diffusion distance of the phase-transition gas and the methane concentration, the damaged LNG carrier in a head and following wind would undergo the same level of risk.

Fig. 30 compares the temperature fields on the deck and near the cargo tank in Case 3 and Case 4 at different moments, analyzing the effect of the head and following wind on the temperature on the hull surface. From the diffusion range of the cryogenic environment on the deck, the stern deck in the head wind scenario is more vulnerable to the cryogenic phase-transition gas. Meanwhile, the bow deck in the following wind scenario is more vulnerable to the cryogenic phase-transition gas.

The five cargo tanks will be affected to varying degrees from the beginning of the leakage. However, in the middle and later stages of the damage leakage, the cryogenic environment in the head wind scenario will only affect the NO.4 tank at most, and in the following wind scenario will affect the NO.2 tank at most. Overall, the influence range of the cryogenic environment in these two scenarios is concentrated in NO.3 tank with its adjacent NO.2 and NO.4 tanks.

6. Comparison analysis between the no wind and beam wind towards the damaged side

Comparing the research results in Section 5, whether it is the methane concentration or cryogenic diffusion on the hull surface, the beam wind towards the damaged side is the most dangerous condition. To analyze its influence degree more intuitively, Figs. 31 and 32 compare the leakage results with the no wind condition. First, as shown in the methane concentration in Fig. 31, methane only spread on the damaged side when there is no wind. However, beam wind towards the damaged side of the LNG carrier causes the cryogenic methane to spread to the intact side, and the damaged LNG carrier is surrounded by methane on all sides, which will greatly increase the explosion risk. Second, judging from the temperature of the hull surface in Fig. 32, in the absence of wind excitation, the cryogenic diffusion only affects the space around the damaged compartment. However, for the damaged carrier in beam winds towards the damaged side, all five cargo compartments are affected by the cryogenic environment. Overall, through the above comparison with the no wind condition, the influence degree of the beam wind towards the damaged side of the LNG carrier to the hull has been further clarified.

7. Conclusions and future work

Damage leakage of an LNG carrier will lead to serious RPT behavior, and the cryogenic diffusion accompanied by the phase-transition gas will significantly affect the safety of the ship structure and the crew on board. To better understand the leakage process and diffusion characteristics of the damaged LNG carrier, this paper numerically simulates the leakage scenarios in four wind directions. The novelty of the study is to replicate the natural leakage of LNG by combining CFD and boiling models. Numerical results can provide a valuable reference for the rescue management, disaster prevention, and structural design of LNG carriers. The main conclusions can be summarized as follows:

(1) For the rescue management, the damaged LNG carrier should maneuver to adjust the relative direction of the hull to the wind as much as possible, and the safe working area is the upwind area. Based on the numerical results in Section 5, the beam wind towards the intact side of the LNG carrier will effectively mitigate the diffusion range of the cryogenic phase-transition gas around the hull, providing a larger operable area for the emergency team.

(2) In terms of disaster prevention, different wind directions do not have a significant effect on the leakage volume. However, to avoid the risk of explosion due to the excessive methane concentration, emergency operators should prevent the damaged LNG carrier from being positioned in the beam wind towards the damaged side.

(3) For the design of low temperature resistance of the ship upper structure, the diffusion of cryogenic gas on the deck will vary depending on the leakage location, damage size, and wind direction Considering that the density of the phase-transition gas is greater than that of air, the sinking phase-transition gas primarily affects the tank area close to the deck. Therefore, it is necessary to provide appropriate cryogenic protection for this area to reduce the risk of cryogenic brittleness to the tank structure.

Moreover, the numerical approach proposed, and the results presented in this paper will further promote safety research on damaged

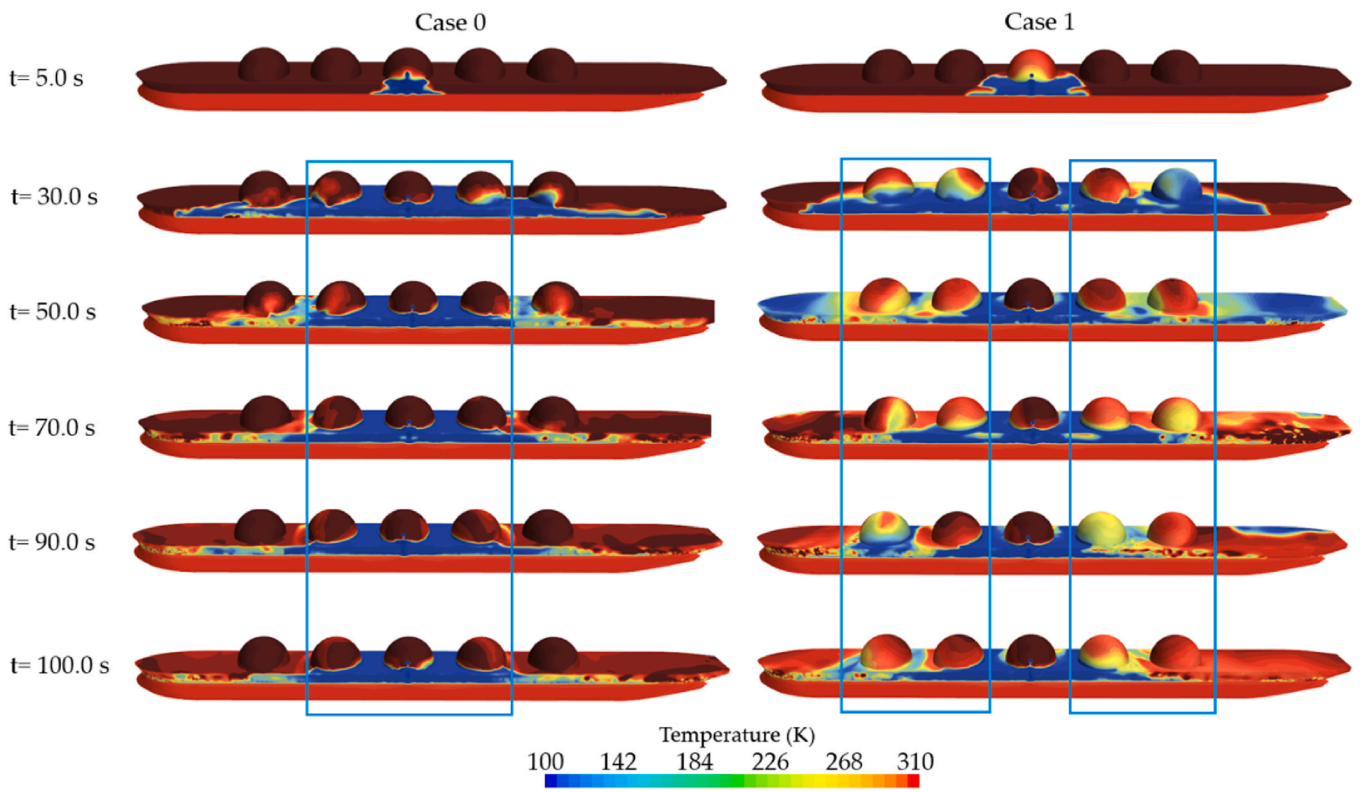

Fig. 32. Temperature comparison on the hull surface between Case 0 and Case 1.

LNG carriers and the design of low temperature service steel of the hull structure. However, there are a few areas that deserve further investigation:

(1) The present study assumes the damaged LNG carrier is stationary. The influence of the vessel's motion will be taken into consideration in future work.
(2) The present study examines the leakage characteristics of the damaged LNG carrier in still water. External wave excitation will be accounted for in future work.
(3) The analysis focuses only on the regular circular opening in the middle tank above the deck. Further consideration should be given to different damaged locations and opening shapes.
(4) This paper only considers the constant wind speed 4 m/s. The influence of the wind speed on the leakage characteristic will be investigated in future work.

CRediT authorship contribution statement

XinLong Zhang: Writing – original draft, Visualization, Validation, Methodology, Investigation, Formal analysis, Data curation, Conceptualization. **QingYi Qu:** Writing – review & editing, Methodology, Data curation, Conceptualization. **Simone Mancini:** Writing – review & editing, Visualization, Validation, Software, Methodology, Formal analysis. **Li Lin:** Writing – review & editing, Supervision, Resources, Project administration, Funding acquisition. **YiHua Su:** Writing – review & editing, Resources, Project administration. **RenQing Zhu:** Supervision, Resources, Project administration, Funding acquisition, Conceptualization.

Funding

This work was supported by the Natural Science Foundation of Jiangsu Province (Grant No. BK20241016), National Natural Science Foundation of China (Grant No. 52271318) and China Classification Society scientific research project: "Evaluation methods of Type-A containment system of liquefied gas carrier and inspection technology research of prismatic Type-B containment system".

Declaration of competing interest

The authors declare that they have no known competing financial interests or personal relationships that could have appeared to influence the work reported in this paper.

References

Al-Yafei, H., Aseel, S., Kucukvar, M., Kucukvar, M., Onat, N.C., Al-Sulaiti, A., 2021. A systematic review for sustainability of global liquified natural gas industry: a 10-year update. Energy Strategy Rev. 38, 100768.
Choi, S.W., Kim, H.S., Lee, W.I., 2016. Analysis of leaked LNG flow and consequent thermal effect for safety in LNG cargo containment system. Ocean Eng. 113, 276–294.
Cao, Y., Jia, Q.J., Wang, S.M., Jiang, Y., Bai, Y., 2022. Safety design analysis of a vent mast on a LNG powered ship during a low-temperature combustible gas leakage accident. J. Ocean Eng. Sci. 7, 75–83.
George, J.J., Renjith, V.R., George, P., George, A.S., 2019. Application of fuzzy failure mode effect and criticality analysis on unloading facility of LNG terminal. J. Loss Prev. Process. Ind. 61, 104–113.
Giannissi, S.G., Venetsanos, A.G., Markatos, N., Bartzis, J.G., 2013. Numerical simulation of LNG dispersion under two-phase release conditions. J. Loss Prev. Process. Ind. 26 (1), 245–254.
Horvat, A., 2018. CFD methodology for simulation of LNG spills and rapid phase transition (RPT). Process Saf. Environ. Prot. 120, 358–369.
ITTC Procedures and Guidelines, 2011. Practical Guidelines for Ship CFD Applications, 7.5-03-02-03.
Kong, X., Jiao, W., Xiang, W., Wang, W., Wang, Q., Cao, J., Han, L., 2023. Quantitative analysis of leakage consequences of LNG carrier-to-ship bunkering based on CFD. Energies 16, 4631.
Kang, J., Lv, K., Sun, Y., Li, M., 2025. Predictive risk assessment framework for leakage accident of offshore LNG transfer system. Expert Syst. Appl. 271, 126580.
Koopman, R.P., Cederwall, R.T., Ermak, D.L., Goldwire, H.C., Hogan, W.J., McClure, J. W., Shinn, J.H., 1982. Analysis of Burro series 40-m3 lng spill experiments. J. Hazard Mater. 6 (1), 43–83.
Kim, B.K., Mentzer, R.A., Mannan, M.S., 2014. Numerical study on physical mechanisms of forced dispersion for an effective LNG spill mitigation. Ind. Eng. Chem. Res. 53 (22), 9488–9498.

Luketa-Hanlin, A., 2006. A review of large-scale LNG spills: experiments and modeling. J. Hazard Mater. 132 (2–3), 119–140.
Nubli, H., Jung, D., Kim, S.J., Sohn, J.M., 2024. Structural impact under accidental LNG release on the LNG bunkering ship: implementation of advanced cryogenic risk analysis. Process Saf. Environ. 186, 329–347.
Nubli, H., Sohn, J.M., Prabowo, A.R., 2022. Layout optimization for safety evaluation on LNG-fueled ship under an accidental fuel release using mixed-integer nonlinear programming. Int. J. Nav. Archit. Ocean Eng. 14, 100443.
Wu, J., Cai, J., Yuan, S., Zhang, X., Reniers, G., 2021. CFD and EnKF coupling estimation of LNG leakage and dispersion. Saf. Sci. 139, 105263.
Xie, C., Huang, L.W., Wang, R., Deng, J., Shu, Y.Q., Jiang, D., 2022. Research on quantitative risk assessment of fuel leak of LNG-fuelled ship during lock transition process. Reliab. Eng. Syst. Saf. 221.
Yu, J.X., Ding, H.Y., Yu, Y., Wu, S.B., Zeng, Q.Z., Xu, Y., 2024. Risk assessment of liquefied natural gas storage tank leakage using failure mode and effects analysis with Fermatean fuzzy sets and CoCoSo method. Appl. Soft Comput. 154.
Yang, Q., Pan, X., 2015. Application of perturbation method to extended evaporation model of LNG leakage to water surface. Oil Gas Storage Transp. 34 (6), 653–656.
Zhu, G., Guo, X., Yi, Y., Tan, W., Ji, C., 2020. Experimental and simulation research of evolution process for LNG leakage and diffusion. J. Loss Prev. Process. Ind. 64, 104041.
Zhu, R.C., Hu, X.F., Bai, Y.P., Li, X., 2021. Risk analysis of terrorist attacks on LNG storage tanks at ports. Saf. Sci. 137.
Zhang, Z., Zhu, W., Pan, X., Tan, B., Ye, Z., Zhang, L., Zhou, X., Jiang, J., 2024. Field experimental study of high expansion foam coverage after LNG leakage. Process Saf. Environ. 183, 315–326.
Zhang, Y., Zhu, J., Teng, L., Song, C., Li, Y., 2020. Experimental research of LNG accidental underwater release and combustion behavior. J. Loss Prev. Process. Ind. 64, 104036.
Zhang, X.L., Lin, L., Su, Y.H., Ma, S., Wang, G., Mancini, S., 2025. Numerical study on the dynamic RPT behavior of the damaged LPG carrier with combined CFD and VOF boiling model. Ocean Eng. 323, 120546.